AFOSR-TR-97-0381

REPORT DOCUMENTATION PAGE

Form Approved
OMB No. 0704-0188

1. AGENCY USE ONLY (Leave blank)	2. REPORT DATE	3. REPORT TYPE AND DATES COVERED
	July 10, 1997	Final 3/15/94 - 4/14/97

4. TITLE AND SUBTITLE

Numerical Simulations of Wall Jets

5. FUNDING NUMBERS

F49620-94-1-0208

6. AUTHOR(S)

Hermann F. Fasel, Professor

7. PERFORMING ORGANIZATION NAME(S) AND ADDRESS(ES)

Department of Aerospace and Mechanical Engineering
The College of Engineering and Mines
The University of Arizona
Tucson, AZ 85721

8. PERFORMING ORGANIZATION REPORT NUMBER

9. SPONSORING / MONITORING AGENCY NAME(S) AND ADDRESS(ES)

AFOSR/NA
110 Duncan Avenue, Room B115
Bolling AFB, DC 20332-8080

NA

10. SPONSORING / MONITORING AGENCY REPORT NUMBER

11. SUPPLEMENTARY NOTES

12a. DISTRIBUTION / AVAILABILITY STATEMENT

Approved for Public Release
Distribution is Unlimited

12b. DISTRIBUTION CODE

13. ABSTRACT (Maximum 200 words)

This document summarizes the three year investigation of transitional and turbulent wall jets using direct numerical simulation (DNS) and large eddy simulation (LES). Towards this end, a three-dimensional, incompressible Navier-Stokes code developed in our research group for DNS of boundary-layer transition was adapted to the wall jet geometry. The code is based on the spatial model and is fourth-order accurate. For the LES, a Smagorinsky based subgrid-scale turbulence model and explicit fourth-order accurate compact filtering were incorporated. As an initial condition, a base flow close to Glauert's similarity solution of the laminar wall jet was employed. This flow was forced by blowing and suction through a slot in the wall. Periodic forcing was used for investigating primary and secondary instabilities in transitional wall jets ($Re_{\delta m}$=200). We discovered competing two-dimensional (2-D) and three-dimensional (3-D) instability mechanisms which can be influenced significantly by the type of forcing. 2-D large-amplitude forcing produces (2-D) large coherent structures which reduce wall shear but may lead to ejections of vortices from the wall and even to a detachment of the wall jet. Additional 3-D forcing weakens these coherent structures (especially in the near-wall region) and can thus prevent vortex ejections. In our LES of turbulent wall jets, rapid breakdown to turbulence was triggered by large-amplitude 3-D random forcing. Despite the purely 3-D forcing, 2-D coherent structures still emerge in the free shear layer-like outer region, an indication of the strong 2-D instability of the wall jet. A fully turbulent mean flow which compares well with experiments is obtained for higher Reynolds numbers ($Re_{\delta m}$=2000).

14. SUBJECT TERMS

15. NUMBER OF PAGES
28

16. PRICE CODE

17. SECURITY CLASSIFICATION OF REPORT	18. SECURITY CLASSIFICATION OF THIS PAGE	19. SECURITY CLASSIFICATION OF ABSTRACT	20. LIMITATION OF ABSTRACT
UNCLASSIFIED	UNCLASSIFIED	UNCLASSIFIED	Unlimited

NUMERICAL SIMULATION OF WALL JETS

AFOSR Grant Number F49620-94-1-0208

Final Report

by

Hermann F. Fasel
Department of Aerospace and Mechanical Engineering
The University of Arizona
Tucson, AZ 85721

Submitted to

The Air Force Office of Scientific Research

May 1997

Final Report

NUMERICAL SIMULATION OF WALL JETS

AFOSR Grant Number F49620-94-1-0208

Principal Investigator
Hermann F. Fasel
Department of Aerospace and Mechanical Engineering
The University of Arizona
Tucson, AZ 85721

ABSTRACT

This document summarizes the three year investigation of transitional and turbulent wall jets using direct numerical simulation (DNS) and large eddy simulation (LES). Towards this end, a three-dimensional, incompressible Navier-Stokes code developed in our research group for DNS of boundary-layer transition was adapted to the wall jet geometry. The code is based on the spatial model and is fourth-order accurate. For the LES, a Smagorinsky based subgrid-scale turbulence model and explicit fourth-order accurate compact filtering were incorporated. As an initial condition, a base flow close to Glauert's similarity solution of the laminar wall jet was employed. This flow was forced by blowing and suction through a slot in the wall. Periodic forcing was used for investigating primary and secondary instabilities in transitional wall jets ($Re_{\delta_m} \approx 200$). We discovered competing two-dimensional (2-D) and three-dimensional (3-D) instability mechanisms which can be influenced significantly by the type of forcing. 2-D large-amplitude forcing produces (2-D) large coherent structures which reduce wall shear but may lead to ejections of vortices from the wall and even to a detachment of the wall jet. Additional 3-D forcing weakens these coherent structures (especially in the near-wall region) and can thus prevent vortex ejections. In our LES of turbulent wall jets, rapid breakdown to turbulence was triggered by large-amplitude 3-D random forcing. Despite the purely 3-D forcing, 2-D coherent structures still emerge in the free shear layer-like outer region, an indication of the strong 2-D instability of the wall jet. A fully turbulent mean flow which compares well with experiments is obtained for higher Reynolds numbers ($Re_{\delta_m} \approx 2000$).

INTRODUCTION

The objective of this three year investigation has been to identify and understand the relevant mechanisms that govern the evolution and the dynamical behavior of large (coherent) structures in wall jets in view of applying wall jets efficiently to such tasks as boundary layer control or surface cooling. For achieving this goal, transitional and turbulent wall jets were investigated using direct numerical simulations (DNS) and large eddy simulations (LES). This approach enabled us to study nonlinear mechanisms in wall jets in greater detail than experiments and with greater realism than previous linear studies. A major emphasis of this work was investigating primary and secondary instabilities in transitional wall jets using DNS. Our strong belief is that the instability mechanisms that generate large coherent structures in transitional wall jets are also present in turbulent wall jets. We therefore studied these instability mechanisms, individually and in combination, for a periodically forced transitional wall jet at a low Reynolds number, where DNS can be used as an efficient tool for numerical experiments. For studying turbulent wall jets at higher Reynolds numbers, LES was employed as the more cost effective approach.

CODE DEVELOPMENT AND CODE VALIDATION

Based on our research over many years of numerical simulations of transitional flows, we have developed highly accurate and efficient Navier-Stokes codes [see for example Fasel (1990), Meitz (1996)] that are now tailored for DNS and LES of wall jets.

Features of the Navier-Stokes Code

The code is based on the complete incompressible Navier-Sokes equations in a vorticity-velocity formulation and is based on a spatial model (Fasel 1990). The numerical scheme employs a fourth-order Runge-Kutta method for the time integration, fourth-order accurate compact differences in the streamwise and the wall-normal directions, and a pseudo-spectral approximation in the spanwise direction.

Typically, using the two-dimensional version of the code, a two-dimensional steady base flow is computed first. As an example of a laminar wall-jet base flow, the numerical solution [which is very close to Glauert's (1956) similarity solution] is given in Figure 1. For investigations of transition or for investigating the effects of periodic forcing, this base flow is then disturbed (two-dimensionally and/or three-dimensionally) by blowing and suction through a slot in the wall near the inflow boundary of the computational domain (Figure 1). An example of the streamwise and temporal variation of the wall-normal velocity over the blowing and suction slot is given in Figure 2. The introduced disturbances may grow in the downstream direction and (in the case of three-dimensional forcing) may lead to transition to turbulence. To avoid upstream feed back of the outflow boundary, the flow is relaminarized in a buffer domain close to the outflow with a technique similar to that proposed by Kloker et al. (1993).

Code Improvements for DNS

Over the past three years, major improvements have been made that considerably increased the efficiency for computing wall-jet flows. Towards this end, we have implemented the capability of using variable grid spacing in the wall-normal direction. This is crucial for computing turbulent flows due to the wide range of scales in the wall-normal direction that have to be resolved in the simulations. Along the variable grid, the coefficients in the compact difference stencils are adjusted such that fourth-order accuracy is maintained. Our approach gives more accurate results than grid transformation methods.

For computations with a high wall-normal resolution, the time step in the explicit scheme is limited due to numerical instabilities caused by the wall-normal diffusion terms in the vorticity transport equations. By treating these terms implicitly, we were able to speed up the time integration by a factor of four when compared to the fully explicit fourth-order Runge-Kutta method.

Code Validation for DNS

We validated our DNS code for boundary-layer transition by comparing benchmark calculations of primary and secondary instability to results obtained with a nonlinear PSE solver that we developed

(Schwolow 1994). Excellent agreement was found for all two-dimensional and three-dimensional, linear and nonlinear computations.

For transitional wall jets, we compared our DNS results to linear stability theory (LST). We found excellent agreement for both velocity profiles and growth rates when forcing only the inner mode (Wernz 1993). For a combination of both modes, we applied a decomposition method proposed by Thumin et al. (1996) to determine the contributions from the inner and the outer mode to the DNS result. Some results obtained with this method are discussed in our attached AIAA paper (Wernz and Fasel 1997).

Code Development for LES

A subgrid-scale turbulence model was implemented into the Navier-Stokes DNS code and tested first for a flat-plate boundary layer and then for a wall jet. As a first step, we chose a basic Smagorinsky-type subgrid-scale model suggested by Speziale, (Personal Communication, 1995). In this model, the Smagorinsky coefficient, which was first calibrated for a boundary-layer flow, is the only modelling coefficient.

In the past, LES was carried out with, at most, second-order accuracy (often combined with inadequate filtering techniques). This resulted in a co-mingling of numerical errors (truncation error) with the effects of the subgrid-scale model. In contrast, in our LES, we are employing fourth-order accurate compact differences with spectral-like resolution (Lele 1992) and fourth-order accurate compact filters. We have insisted on fourth-order accuracy for the spatial discretization and for filtering since this allows a clean separation of the resolved scales (computed by Navier-Stokes) and the unresolved scales (modeled by subgrid-scale model). This approach will facilitate an objective evaluation of the performance of the improved subgrid-scale models that we plan to implement and test in the future.

We were able to carry out "fully" transitional simulations (i.e., computing through transition all the way from laminar to turbulent flow [1]) by using a spectral ramping function which turns on the subgrid-scale model when the fluctuation level surpasses a specified threshold in a (specified) high spanwise Fourier component (e.g., k=10).

We have found efficient techniques to "turn-on" or "trigger" turbulence for DNS and LES of turbulent flows using, for example, "bypass transition" initiated by random forcing of purely oblique modes (spanwise Fourier components k=1 and k=2) with forcing introduced by blowing and suction (see Figure 1). An example of some typical random time signals is given in Figure 3. We found this method to be very effective for rapid transition to turbulence, thus providing a good match of the turbulence statistics (turbulent mean flow, skin friction, rms-values) to experimental measurements early on in the turbulent flow regime.

Code Validation for LES

For validation of the LES code (including the subgrid-scale model), we used a flat-plate boundary layer because, for this flow, a wealth of experimental and numerical data is available for comparison. With our LES code, we performed calculations of bypass transition using the random forcing method mentioned above. We then compared our results with those from a DNS by Rai and Moin (1991)

[1] This is not to say our current subgrid-scale model (equilibrium turbulence model) is already adequate in the transitional flow regime (non-equilibrium).

and from experiments by Suder et al. (1988). Typical results of these comparison calculations are presented in Figures 4-6:

An impression of the flow field for a typical case (Case 1) is given in Figure 4, which displays a snapshot at one time instant of the two-dimensional Fourier component (k=0) of the spanwise vorticity. In Figure 5, the mean flow profiles of the u-velocity and the Reynolds stresses for this case are shown in wall coordinates for different downstream locations in the transitional region. Both the u-velocity profiles and the Reynolds stresses quickly approach the shapes that appear in a turbulent boundary layer.

In Figure 6, the skin-friction coefficient is plotted versus the streamwise coordinate for two cases of our LES calculations with different forcing amplitudes. Comparison is made to the DNS and experimental measurements. During transition, the skin-friction coefficient of LES Case 1 (larger amplitude) closely follows that of the experiment, while the skin-friction coefficient of LES Case 2 (smaller amplitude) closely follows that of the DNS. In both cases, however, very good agreement was reached at the end of the transition region (for the skin-friction coefficients, spreading rate, mean flow profiles, rms-values, and Reynolds stress). These calculations have shown that, with our subgrid-scale model and with the random forcing method (modeling bypass transition), we are able to effectively "trigger" turbulent flow and quickly arrive at realistic turbulent flow quantities.

After completing the validation calculations for the flat-plate boundary layer, we have also performed validation calculations for a case of bypass transition for a wall jet. Figure 7 shows the instantaneous flow field (Fourier component k=0 of the spanwise vorticity) for a typical case. In Figure 8, the mean flow profiles of the u-velocity (normalized with local velocity maximum and half width) are shown for different downstream locations in the transitional region. A clear trend towards the shape of a fully turbulent profile can be observed. We can also observe good agreement with the experimental results by Wygnanski et al. (1992) for the spreading rate (half width) and the decay of the u-velocity maximum (see Figure 9a,b).

However, the comparison with experiments should only be considered qualitative for this case as the Reynolds numbers of the experiments ($Re_{\delta_{max}} > 1500$) is considerably higher than that of the simulation ($Re_{\delta_{max}} \approx 200$, Figure 9c). The difference in Reynolds number might be the reason for the discrepancy in Figure 8 between the mean flow profiles in the near-wall region. Another possiblity is that the Smagorinsky coefficient has to be recalibrated for the wall jet flow. (Turbulent intensity has a greater influence in the inner region than in the outer region.)

To determine the influence of the Reynolds number on the mean flow, we recently started investigating wall jets at Reynolds numbers that are ten times higher ($Re_{\delta_{max}} > 2000$). At these Reynolds numbers, the flow transitions very rapidly and reaches the turbulent flow regime at about the midpoint of the computational domain, as illustrated in Figures 10 and 11 for a typical case. Figure 10 displays the instantaneous flow field (Fourier component k=0 of the spanwise vorticity). Figure 11a shows the mean flow profiles of the u-velocity (again normalized with local velocity maximum and half width) for different downstream locations. For streamwise locations $x > 335$, the shape of a fully turbulent mean flow profile is matched very closely, especially in the inner region, which is in contrast to the low Reynolds number cases we have investigated previously. We therefore conclude that the shape difference between simulation and experiment observed in those cases is likely due to the difference in the Reynolds number, not due to the turbulence model.

While the turbulent mean flow is reproduced well with the current LES, a considerable discrepancy between simulation and experiment exists in the rms-values value of the streamwise velocity (Figure 11b), especially in the outer (shear layer) region of the wall jet. Investigations are under

way to determine the cause for this discrepancy, in particular the role of the subgrid-scale model. We consider implementing a dynamic subgrid-scale model [similar to the one proposed by Germano et al. (1991)] where the Smagorinsky coefficient can be adjusted in wall-normal direction.

SUMMARY OF RESEARCH ACCOMPLISHMENTS

A summary of the work performed and of the accomplishments over the past three years is given here. Typical results and more details are provided in the Appendix.

Meanflow Distortion due to Large Amplitude Forcing

Our simulations confirmed the experimental findings by Zhou et al. (1992) concerning the distortion of the mean flow (decrease of wall shear and velocity maximum, increase of spreading rate) for large amplitude forcing (due to nonlinear interaction of the disturbance with itself).

Two-Dimensional Resonance in a Transitional Wall Jet

We investigated a two-dimensional secondary instability, which is the underlying mechanism for the "vortex merging" observed in experiments on transitional wall jets. We demonstrated that the "vortex merging" is a manifestation of two-dimensional subharmonic resonances that occur in wall jets in a fashion similar to a free shear layer. We studied in great detail a surprising phenomenon caused by this subharmonic resonance: the ejection of mushroom-shaped vortices from the wall jet layer. Results are presented in two attached papers (Wernz and Fasel 1996, Fasel and Wernz 1996).

Three-Dimensional Resonances in a Transitional Wall Jet

We also investigated the three-dimensional breakdown process based on the two "classical" types of (three-dimensional) secondary instability mechanisms: fundamental resonance and subharmonic resonance. We demonstrated that combinations between two-dimensional and three-dimensional resonances are likely to occur in wall jets. We performed detailed paramenter studies on the influence of the disturbance amplitude and the spanwise wavenumber. Results of these investigations are presented in an attached paper (Wernz and Fasel 1997).

LES Computations with Random Forcing

We performed LES computations for turbulent wall jets where turbulence is "triggered" by three-dimensional random forcing (bypass transition). We obtained two-dimensional coherent structures in the flow similar to those observed in experiments on natural transition in wall jets (Bajura and Catalano 1975).

Wall Jets with an External Stream

We investigated the influence of a (weak) external stream on the transition process. We found that an external stream de-emphasizes primary and secondary instabilities associated with the outer (shear layer) region of the wall jet. We performed two-dimensional computations of laminar wall jets in external stream. It was found that ejected vortices are (mostly) convected downstream and provide little upstream feedback.

CONCLUSION AND OUTLOOK

With our investigation of transitional wall jets using DNS, we have gained insight into a flow whose dynamical behavior proved even more complex and interesting that we had anticipated, in particular, the competition and interplay of two-dimensional and three-dimensional resonances and the important role of the three-dimensional resonances for the stability of the observed two-dimensional large coherent structures.

For the simulation of turbulent wall jets using LES, several improvements and additions to our computational approach are currently being made within the continuation of this project which will greatly enhance efficiency and accuracy of the simulations. These ongoing efforts include: incorporating into our code the capability of continuation calculations with grid refinement in all spatial directions, incorporating a dynamical subgrid-scale model which can adjust over the inner and the outer region of the wall jet, and improving our toolkit for analyzing the mixture of periodic and random fluctuations in periodically forced turbulent wall jets.

PERSONNEL

Hermann F. Fasel, professor, principal investigator,
Stefan Wernz, graduate student.

PUBLICATIONS

Wernz, S. and Fasel, H., 1996, "Vortex Motion in an Unsteady Forced Wall Jet," *Phys. Fluids*, Vol. 8, No. 9, p. S11.

PRESENTATIONS AT CONFERENCES

Fasel, H. and Wernz S., "Numerical Simulation of a Forced Laminar Wall Jet," *APS*, 48th Annual Meeting of the Division of Fluid Mechanics, Irvine, CA, Nov. 19-21, 1995.

Wernz, S. and Fasel, H., "Numerical Simulation of the Three-Dimensional Stages of Transition in a Laminar Wall Jet," *APS*, 48th Annual Meeting of the Division of Fluid Mechanics, Irvine, CA, Nov. 19-21, 1995.

Wernz, S. and Fasel, H., "Numerical Investigation of Unsteady Phenomena in Wall Jets," 34th AIAA Aerospace Sciences Meeting and Exhibit, Reno, NV, Jan. 15-18, 1996.

Fasel, H. and Wernz S., "Numerical Simulation of Wall Jets," 3rd International Symposium on Engineering Turbulence Modelling and Measurements, Heraklion-Crete, Greece, May 27-29, 1996.

Fasel, H. and Wernz S., "Large Eddy Simulation of Transitional and Turbulent Wall Jets," *APS*, 49th Annual Meeting of the Division of Fluid Mechanics, Syracuse, NY, Nov. 24-26, 1996.

Wernz, S. and Fasel, H., "Numerical Investigation of Forced Transitional Wall Jets," 28th AIAA Fluid Dynamics Conference, Snowmass Village, CO, June 29-July 2, 1997.

REFERENCES

Amitay, M., 1994, "Theoretical and Experimental Investigations of a Laminar Two-Dimensional Wall-Jet," Research thesis, Israel Institute of Technology.

Bajura, R. A. and Catalano, M. R., 1975, "Transition in a Two-Dimensional Plane Wall Jet," *J. Fluid Mech.* **70**, 773-799.

Fasel, H., 1990, "Numerical Simulation of Instability and Transition in Shear Flows," Invited Paper, 3rd IUTAM Symposium on Laminar-Turbulent Transition, Toulouse, France.

Fasel, H., and Wernz, S., 1996, "Numerical Simulation of Wall Jets," in *Engineering Turbulence Modelling and Experiments 3*, (W. Rodi and G. Bergeles, eds.), pp. 621-630, Elsevier.

Germano, M., Piomelli, U., Moin, P. and Cabot, W. H., 1991, "A Dynamic Subgrid-Scale Eddy Viscosity Model," *Phys. Fluids A* **7**, 1760-1765.

Glauert, M.B., 1956, "The Wall Jet," *J. Fluid Mech.* **1**, 625-643.

Kloker, M., Konzelmann, U. and Fasel, H., 1993, "Outflow boundary conditions for spatial Navier-Stokes Simulations of Transitional Boundary Layers," *AIAA J.* **31**, 620-628.

Lele, S. K., 1992, "Compact Finite Difference Schemes with Spectral-like Resolution," *J. Comp. Physics* **103**, 16-42.

Meitz, H., 1996, "Numerical Investigation of Suction in a Transitional Flat-Plate Boundary Layer," PhD Dissertation, University of Arizona.

Rai, M. M., and Moin, P., 1991, "Direct Numerical Simulation of Transition and Turbulence in a Spatially Evolving Boundary Layer," AIAA Paper 91-1607.

Schwolow, R., 1994, "Stability Analysis of Boundary Layer Flows Using the Nonlinear Parabolized Stability Equations," Diploma thesis, University of Stuttgart.

Shih, C. and Gogineni, S., 1995, "Experimental Study of Perturbed Laminar Wall Jet," *AIAA J.* **33**, 559-561.

Suder, K.L., O'Brien, J.E. and Reshotko, E., 1988, "Experimental Study of Bypass Transition in a Boundary Layer," NASA TM-100913.

Thumin, A., Amitay, M., Cohen, J. and Zhou, M. D., 1996, "A Normal Multi-Mode Decomposition Method For Stability Experiments," *Phys. Fluids* **8**, 2777-2779.

Wernz, S., 1993, "Stability Investigations of a Laminar Wall Jet Using the Linear Stability Theory," Master's thesis, University of Arizona.

Wernz, S. and Fasel, H., 1996, "Numerical Investigation of Unsteady Phenomena in Wall Jets," AIAA Paper 96-0079.

Wernz, S. and Fasel, H., 1996, "Vortex Motion in an Unsteady Forced Wall Jet," *Phys. Fluids*, Vol. 8, No. 9, p. S11.

Wernz, S. and Fasel, H., 1997, "Numerical Investigation of Forced Transitional Wall Jets," AIAA Paper 97-2022.

White, F.M., 1974, *Viscous Fluid Flow*, McGraw-Hill.

Wygnanski, I., Katz, Y. and Horev, E., 1992, "On the Applicability of Various Scaling Laws to the Turbulent Wall Jet," *J. Fluid Mech.* **234**, 669-690.

Zhou, M. D., Rothstein, J. and Wygnanski, I., 1992, "On the Hydrodynamic Stability of the Wall-Jet," in *Proceedings of the 11th Australasian Fluid Mechanics Conference*, pp. 407-410.

APPENDIX: RESEARCH ACCOMPLISHMENTS

During each stage of our code development effort, we performed numerous simulations with our DNS code of forced transition to turbulence in wall jets. The objective of these investigations was to identify the key mechanisms during forced transition and to explore in detail nonlinear phenomena that may also be relevant for fully turbulent wall jets. The knowledge obtained from the transition investigations was also very helpful for our LES of turbulent wall jets for determining efficient ways to "trigger" transition in order to reach the turbulent regime as quickly as possible.

Meanflow Distortion due to Large Amplitude Forcing

During the first stage of our investigations, we focused on gaining an understanding of the nonlinear effects of two-dimensional large-amplitude forcing that have been observed in experiments of transitional wall jets and could not be explained by linear stability theory. One important nonlinear effect we observed was the distortion of the mean flow such that the spreading rate of the wall jet was increased and both the velocity maximum and the wall shear were decreased. The mean flow distortion can be directly attributed to nonlinear interactions of the fundamental disturbance with itself. For a typical streamwise location, Figure 12 shows the percentile decrease of the mean flow velocity maximum, the increase of its wall-normal location, and the decrease of the wall shear as a function of the local amplitude of the fundamental disturbance. An increase of the local disturbance amplitude by one order of magnitude results in a percentile change of these mean flow quantities by two orders of magnitude (as can be expected from nonlinear interactions of sinusoidal travelling waves). Our numerical results are in very good agreement with experiments on a forced transitional wall jet by Zhou et al. (1992).

Two-Dimensional Resonance in a Transitional Wall Jet

A second important nonlinear phenomenon that we studied in great detail is the two-dimensional subharmonic resonance observed in several experiments on transitional wall jets (Bajura and Catalano 1975, Amitay 1994, Shih and Gogineni in 1995). This two-dimensional secondary instability mechanism is a manifestation of the relationship of wall jets to free shear layers, where the same type of instability mechanism exists. A typical example of a subharmonic resonance observed in our numerical simulations is given in Figure 13. Shown is the instantaneous vorticity field for a case of large-amplitude forcing with a fundamental frequency ($A = 0.5\%$, $f = 56Hz$) and simultaneous small-amplitude forcing with a subharmonic frequency ($A = 0.001\%$, $f = 28Hz$). Halfway through the downstream extent of the domain shown in Figure 13, merging of subsequent vorticity maxima occurs and, as a consequence, the fluctuation frequency is cut in half. The underlying resonance mechanism can be demonstrated nicely with a Fourier decomposition of the time-periodic disturbance flow. Figure 14 displays, on a logarithmic scale, the Fourier amplitudes of the wall vorticity of the fundamental and subharmonic disturbances for various forcing amplitudes of the fundamental disturbance (A_{fund} = 0.1% - 0.8%). The forcing amplitude of the subharmonic is kept constant ($A_{subh} = 0.001\%$). For forcing amplitudes of the fundamental above $A = 0.3\%$, small subharmonic disturbances grow rapidly up to a large amplitude level due to a resonance with the fundamental. A more detailed discussion of this subharmonic resonance mechanism is given in the attached paper,

"Numerical Investigation of Unsteady Phenomena in Wall Jets", which was presented at the AIAA conference in Reno (Wernz and Fasel 1996).

In our numerical simulations, the subharmonic resonance led to a surprising phenomenon during the startup of periodic forcing – the ejection of mushroom-shaped vortices. This phenomenon has been observed in many experiments on forced transition (Bajura and Catalano 1975, Amitay 1994, Shih and Gogineni 1995) but has never before been investigated numerically. Results of these numerical investigations are discussed in the attached papers; for the startup of periodic forcing in the AIAA paper (Wernz and Fasel 1996), and for a wall jet disturbed by a wave packet in the proceedings of the symposium on "Engineering Turbulence Modelling and Experiments" (Fasel and Wernz 1996).

Three-dimensional Resonances in a Transitional Wall Jet

Experiments by Amitay (1994) have shown that, at lower Reynolds numbers, the transition process was dominated by a two-dimensional subharmonic cascade with the ejection of mushroom shaped vortices. However, at higher Reynolds numbers, this cascade was not observed. Rather, breakdown occurred very quickly in a three-dimensional fashion. Since the near-wall region of the wall jet resembles a boundary layer, it should be expected that, in addition to the two-dimensional subharmonic resonance, three-dimensional resonances similar to the secondary instability of a flat-plate boundary layer can contribute to the transition process as well. While experimentalists (Bajura and Catalano 1975, Amitay 1994, Shih and Gogineni 1995) have investigated the vortex merging due to the two-dimensional secondary instability in some detail, we are not aware of any experimental (or numerical) work on three-dimensional secondary instabilities in wall jets. Since our three-dimensional pseudo-spectral DNS code (see above) is perfectly suited for three-dimensional secondary instability investigations, we have also focused on exploring the three-dimensional breakdown process.

In these DNS, in addition to a large-amplitude two-dimensional disturbance wave, a pair of small-amplitude oblique disturbance waves was also introduced. We have studied two "classical" types of secondary instability mechanisms: fundamental resonance, where the oblique waves have the same frequency as the two-dimensional disturbance wave, and subharmonic resonance, where the oblique waves have half that frequency.

Typical results of these investigations are presented in Figure 15 (three-dimensional fundamental resonance) and in Figure 16 (three-dimensional subharmonic resonance). On the left side of Figures 15 and 16, contour plots are shown for the instantaneous spanwise vorticity of the two-dimensional Fourier component (top) and of the first spanwise Fourier component (bottom). In the graphs on the right side, the wall vorticity amplitudes of both Fourier components are plotted versus the streamwise distance for various forcing amplitudes of the two-dimensional component. In all cases the forcing amplitude of the three-dimensional component is kept fixed at 0.001%. As seen from Figure 15, fundamental resonance occurs for two-dimensional forcing amplitudes of 0.3% and above, which is comparable to the amplitude level required for two-dimensional subharmonic resonance. Therefore, combinations of three-dimensional fundamental and two-dimensional subharmonic resonances are possible. In contrast, as shown in Figure 16, three-dimensional subharmonic resonance occurs already at the lower amplitude level of 0.2% where two-dimensional subharmonic resonance does not yet occur.

Adding all spanwise Fourier components provides an overall view in the physical domain of the

consequence of the secondary instability process. Figures 17-19 display the flow fields for three resonance calculations (with ten spanwise Fourier components): in Figure 17 a three-dimensional fundamental resonance, in Figure 18 the combination between a three-dimensional fundamental resonance and a two-dimensional subharmonic resonance, and in Figure 19 a three-dimensional subharmonic resonance. Shown are iso-surfaces of the spanwise vorticity over two spanwise wavelengths. For the left portion of these perspective plots (when looking in streamwise direction), the top layer of negative vorticity has been removed to expose the layer of positive vorticity below. Also plotted in each case is a top view of the instantaneous spanwise vorticity at the wall, illustrating the variation in spanwise direction. In all three cases, the flow develops in streamwise direction from a purely two-dimensional to a strongly three-dimensional behavior. However, the three-dimensional stage is different for each resonance type. For the fundamental resonance (Figure 17), a strong steady streamwise structure can be observed in the outer region that is periodic in spanwise direction. This structure is associated with Fourier mode [0,1] and is characteristic for fundamental resonance. The same structure also exists for the combined resonance (Figure 18). However, (comparing Figure 18 to Figure 17) the structures closer to the wall, as well as the wall vorticity, show a strong influence of the two-dimensional subharmonic, with a doubling of the dominant streamwise wavelength. It is important to note that in both cases all spanwise variations are aligned in the streamwise direction. This is different for the three-dimensional subharmonic resonance, as shown in Figure 19. Here, the structures show a staggered pattern, which is characteristic for subharmonic resonance in a flat-plate boundary layer as well.

We also performed parameter studies on the dependence of the three-dimensional resonances on the spanwise wavenumber. We found that maximum amplification occurs for the three-dimensional subharmonic resonance when the streamwise wavenumber is about twice the spanwise wavenumber. This is in contrast to three-dimensional fundamental resonance, for which maximum amplification occurs when streamwise and spanwise wavenumbers are about equal. This is very similar to the situation in a flat-plate boundary layer (zero pressure gradient). However, three-dimensional secondary instability mechanisms in a wall jet seem to be more complex. For example, the diagram in Figure 20, which illustrates the dependence of the growth of the first spanwise Fourier component on the spanwise wavenumber for three-dimensional subharmonic instability, shows a second local maximum at a higher wavenumber. It is possible that the wall jet not only has two unstable two-dimensional modes, but also at least two unstable (subharmonic) oblique modes. In a complementary project we plan to compare our DNS results with Thumin's results (Personal Communication 1996), who is currently studying secondary instability mechanisms of the wall jet using weakly nonlinear theory.

With our secondary instability investigations we have demonstrated that, in a wall jet, free shear layer-type transition mechanisms (two-dimensional subharmonic resonance) are competing with boundary layer-type mechanisms (three-dimensional fundamental and subharmonic resonance) allowing a wide range of potential combinations favoring one or the other mechanism. Hence, we were not surprised to encounter combinations of two-dimensional and three-dimensional structures in our recent LES computations of a randomly forced wall jet. We expect such resonances, and in particular the competition of resonance mechanisms, to be relevant as well for turbulent wall jets and for periodically forced wall jets where, dependent on forcing frequencies and receptivity mechanisms, certain resonances can be enhanced over others. In other words, such resonances can possibly be exploited advantageously for flow (separation) control.

LES Computations with Random Forcing

As discussed above, we generate strong three-dimensionality of the transitional flows by randomly forcing with the first and second spanwise Fourier component only. Nevertheless, due to the strong nonlinear interactions at this high level of forcing, a significant two-dimensional Fourier component is generated as well. For very high-amplitude forcing (in the Reynolds number range investigated) the two-dimensional Fourier component develops – probably through a two-dimensional instability mechanism – into organized two-dimensional coherent sturctures in the (free shear layer-like) outer region.

An example of a flow pattern caused by such forcing is shown in Figures 21. In this case, one of the counterclockwise-rotating vortices that develop in the shear layer has eventually lifted off from the wall jet's outer region. It now lingers above the wall jet and keeps growing stronger by entraining vorticity from the wall jet below. However, unlike the ejected vortex pairs in our two-dimensional simulations, the single vortex cannot propel itself further away from the wall since it lacks a strong clockwise-rotating partner from the near-wall region. The lack of strong two-dimensional vortical structures in the near-wall region is probably due to our three-dimensional random forcing method, which mostly triggers three-dimensional instability mechanisms in the near-wall region. These results are particularly exciting because they appear to be consistent with experiments by Bajura and Catalano (1975) on natural transition at moderate Reynolds numbers. They also reported the formation of large vortices in the outer region of the wall jet and a stationary growing vortex right above the wall jet. In the experiments, this vortex eventually grows so strong that it continually lifts off vortices from the inner wall jet layer and ejects them far into the ambient fluid. We plan to repeat our LES simulation of this case with a larger computational domain to confirm these highly important results.

From a different point of view, these results also show that, even when strong three-dimensional structures are present originally, the flow is reorganized in predominantly two-dimensional structures. This, of course, is relevant in the context of flow control using periodic forcing, as dominant two-dimensional structures are much easier to control in practical applications than three-dimensional structures.

Wall Jets with External Stream

For our goal of reaching the turbulent regime efficiently through a rapid transition process, we want to avoid the formation of any vortices lingering above the wall jet (as discussed above) because they would eventually destroy the wall jet flow along the wall. By introducing a small free-stream component, any vortical structures in the outer layer are convected downstream and eventually leave the computational domain. Results of a simulation with a free-stream velocity of about 10% of the wall jet at the outflow are shown in Figure 22. For this flow with an external stream, the forcing amplitude can be many times higher than before without generating stationary vortices in the outer flow. Two-dimensional computations of the startup of periodic forcing also show the fundamental difference in this respect between wall jets with and without a free-stream component. In Figures 23 and 24, the disturbance flow during startup of periodic forcing is compared for two cases with a small free-stream component (Figure 23) and without external stream [2] (Figure 24). While the

[2]This case was presented as a video entry into the "Gallery of Fluid Motion" at the APS meeting in Irvine 1995 (see attached abstract).

initial vortex ejection is very similar in both cases (Figures 23a,b and 24a,b), the upstream motion of ejected vortices is weakened in the presence of an external stream (Figures 23c, 24c). Within 200 forcing periods, all ejected vortex pairs are convected out of the flow domain (Figures 23d, 24d) compared to more than 3000 forcing periods that are required for the case without external stream.

Preliminary calculations have also shown that flow instabilities (primary and secondary) associated with the free shear layer region of the wall jet are de-emphasized with increasing free-stream velocity (as expected).

FIGURES

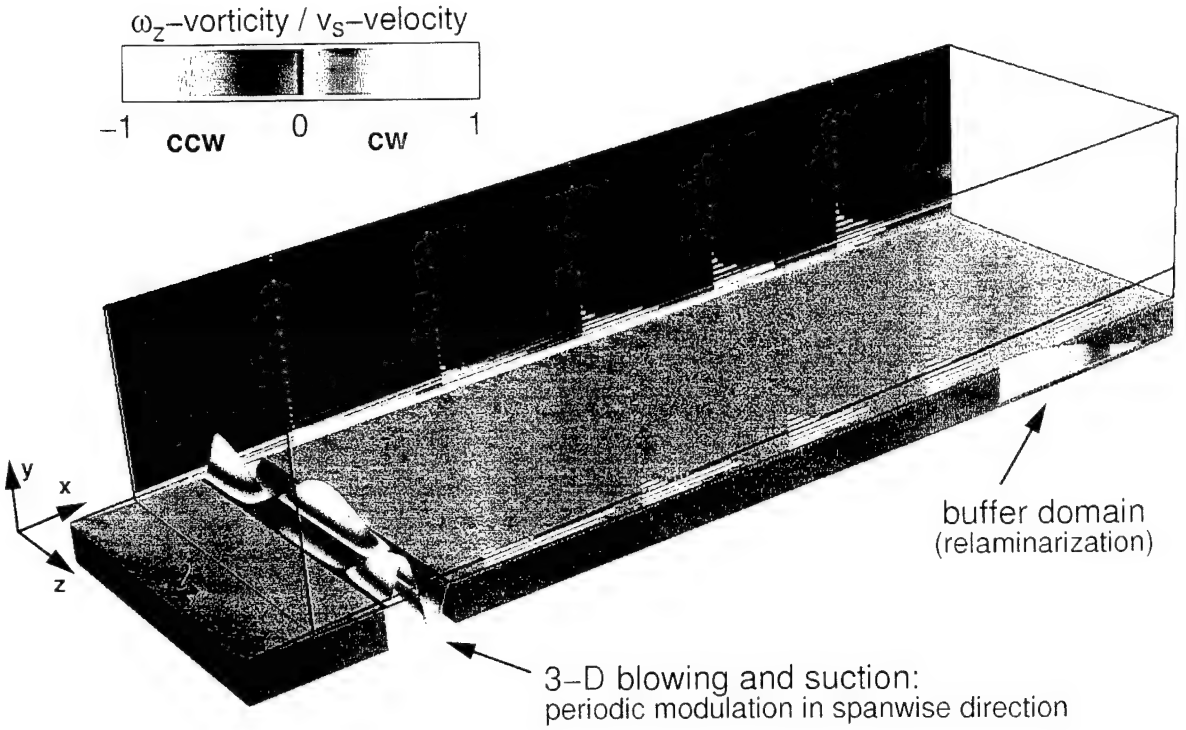

Figure 1: Computational domain in physical space with typical base flow (wall jet with no external stream). The velocity field is represented by vectors and the spanwise vorticity ω_z by color contours. Red indicates clockwise rotation (cw), blue indicates counterclockwise rotation (ccw). Disturbances are introduced by blowing and suction through a slot in the wall, either 2–D or with a spanwise variation (3–D, plot). Before the disturbances can reach the outflow boundary, they are damped out in the buffer domain (relaminarization of the flow).

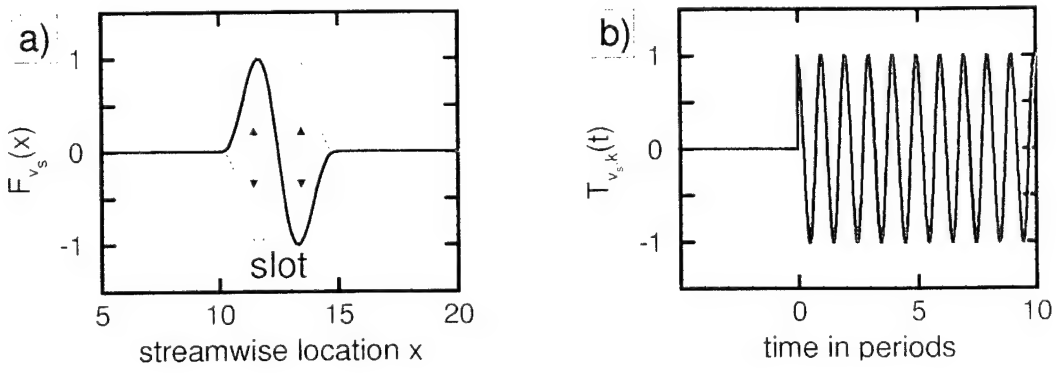

Figure 2: Disturbance generation (forcing) by blowing and suction through a slot in the wall. The flow can be forced in any spanwise Fourier component (for 3–D calculations). The wall–normal velocity over the blowing and suction slot for each spanwise Fourier component is specified by $v_{s,k}(x,t)=A_k*F_{v_s}(x)*T_{v_s,k}(t)$, where A_k represents the forcing amplitude. Shown in a) is the streamwise variation $F_{v_s}(x)$ over the blowing and suction slot, shown in b) is the temporal forcing function $T_{v_s,k}(t)$ of the spanwise Fourier component k. For this example, $T_{v_s,k}(t)=H(t)*\cos(2\pi ft+\phi)$.

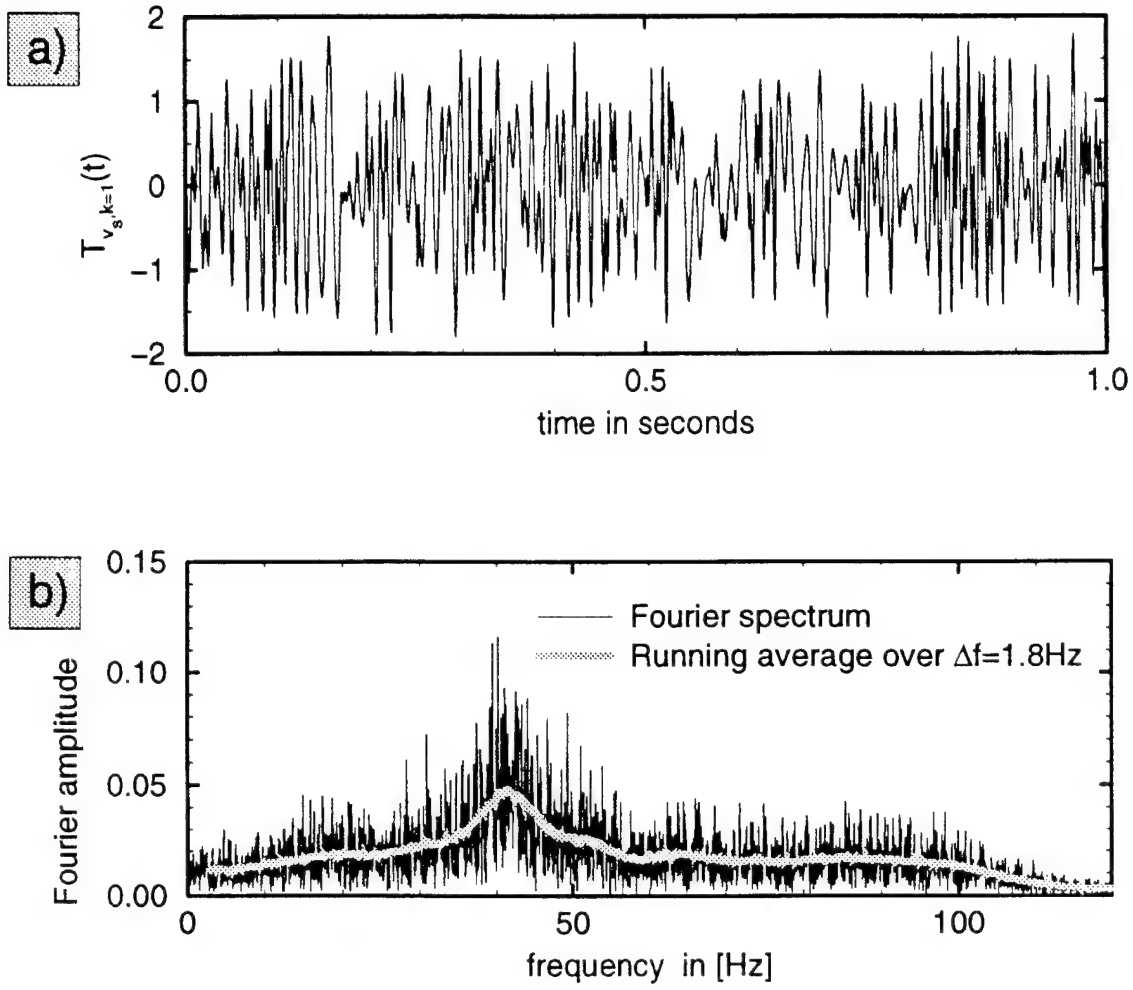

Figure 3: Example of the random forcing method used for triggering bypass transition in the LES computations: a) temporal forcing function $T_{v_s,k=1}(t)$, b) corresponding frequency spectrum.

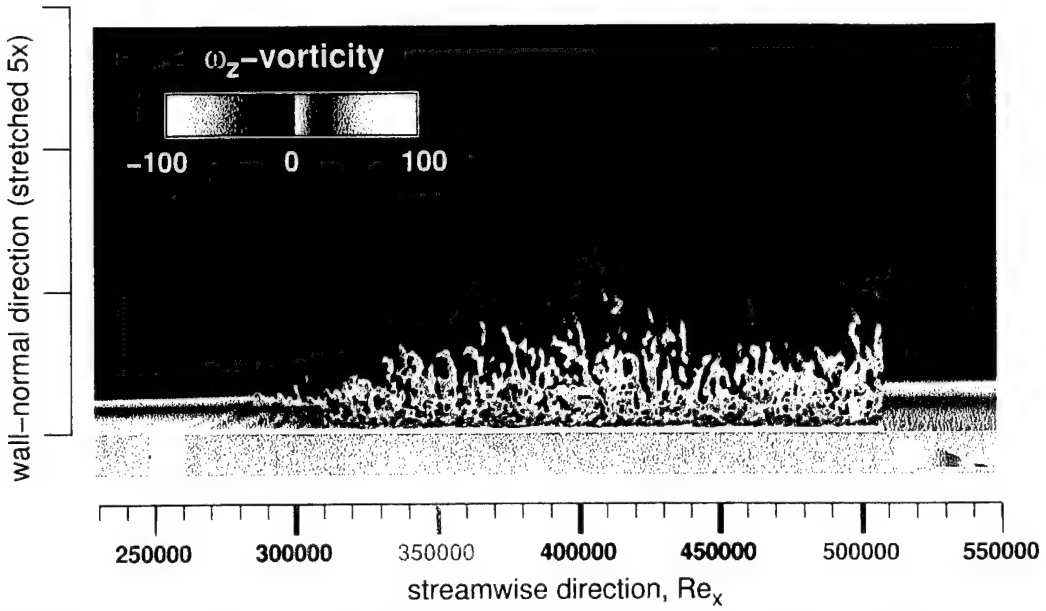

Figure 4: Bypass transition in a flat–plate boundary layer computed with our LES code (Case 1). Shown are color contours of the two–dimensional Fourier component (k=0) of the spanwise vorticity. The flow is disturbed by random forcing (blowing and suction slot) in the first and in the second spanwise Fourier component (k=1,0).

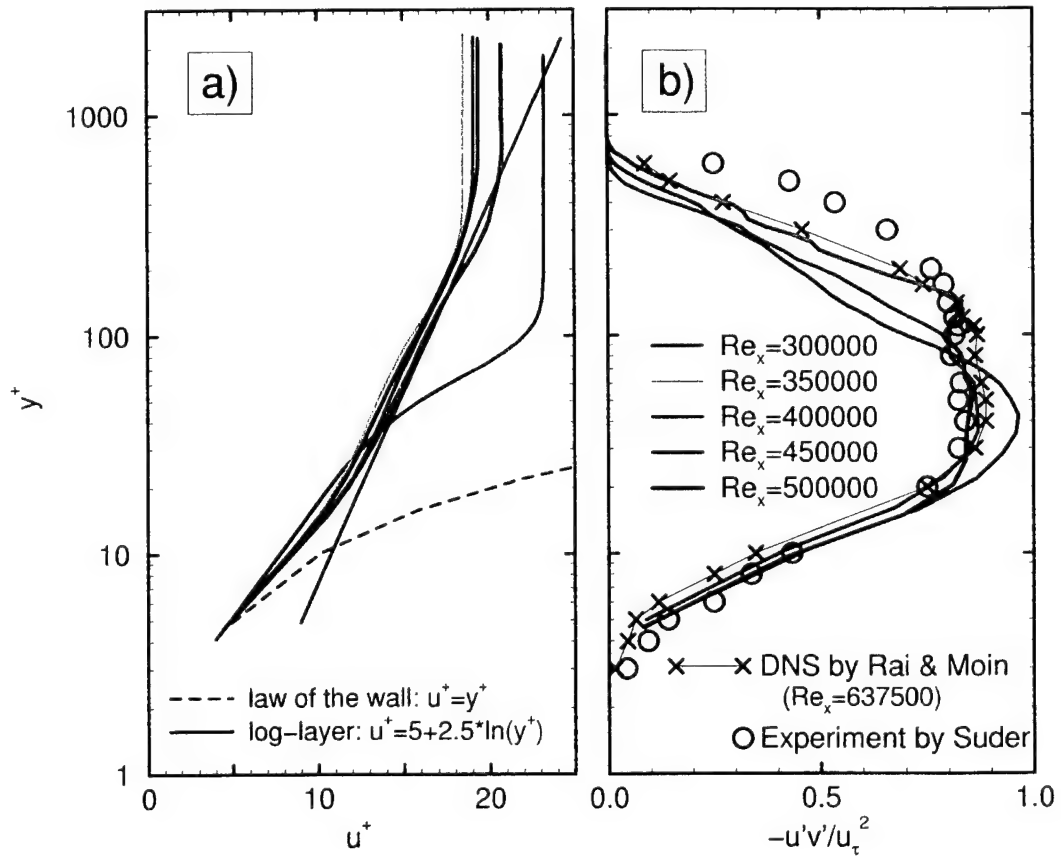

Figure 5: For the LES results shown in Figure 4: a) meanflow velocity profiles, and b) corresponding Reynolds stresses in wall coordinates at five streamwise locations.

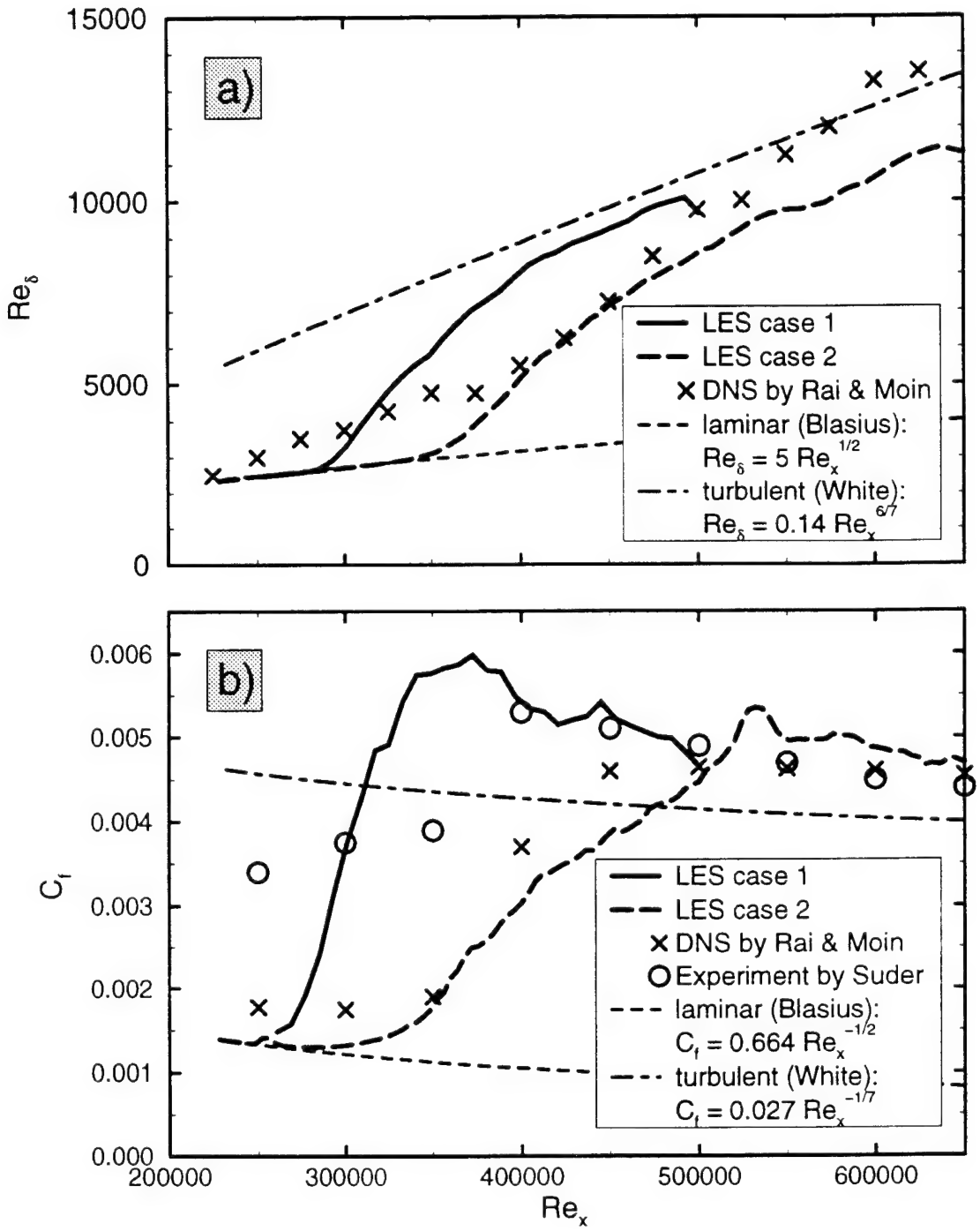

Figure 6: Comparison of our LES results for two cases of bypass transition in a flat plate boundary layer with results from a DNS by Rai and Moin (1991) and with experiments by Suder (1988): a) boundary layer thickness, and b) the skin friction coefficient. For Case 1 of our LES computations stronger forcing was applied than for Case 2.

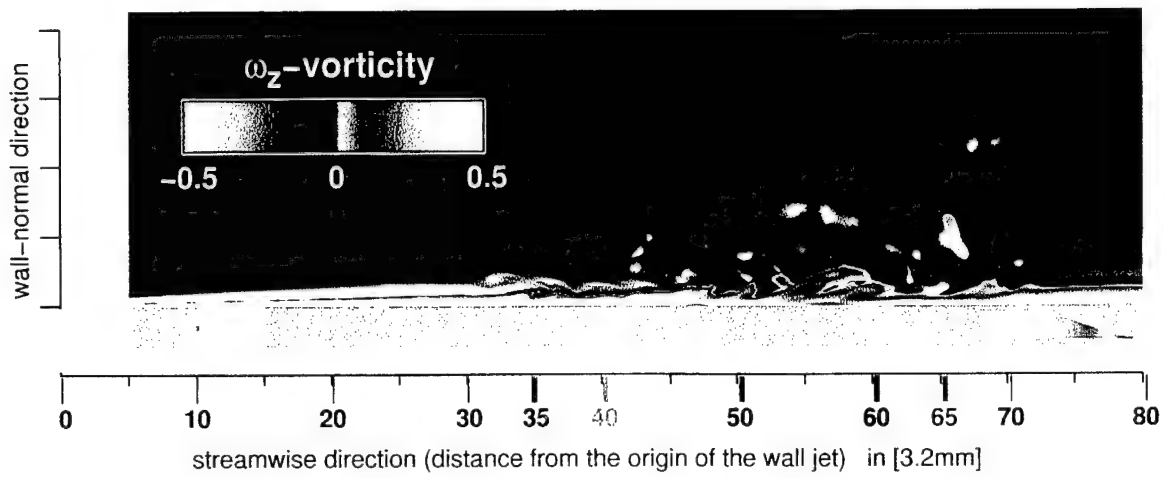

Figure 7: Bypass transition in a wall jet computed with our LES code. Shown are color contours of the two–dimensional Fourier component (k=0) of the spanwise vorticity. The flow is disturbed by random forcing (blowing and suction slot) in the first and in the second spanwise Fourier component (k=1,0).

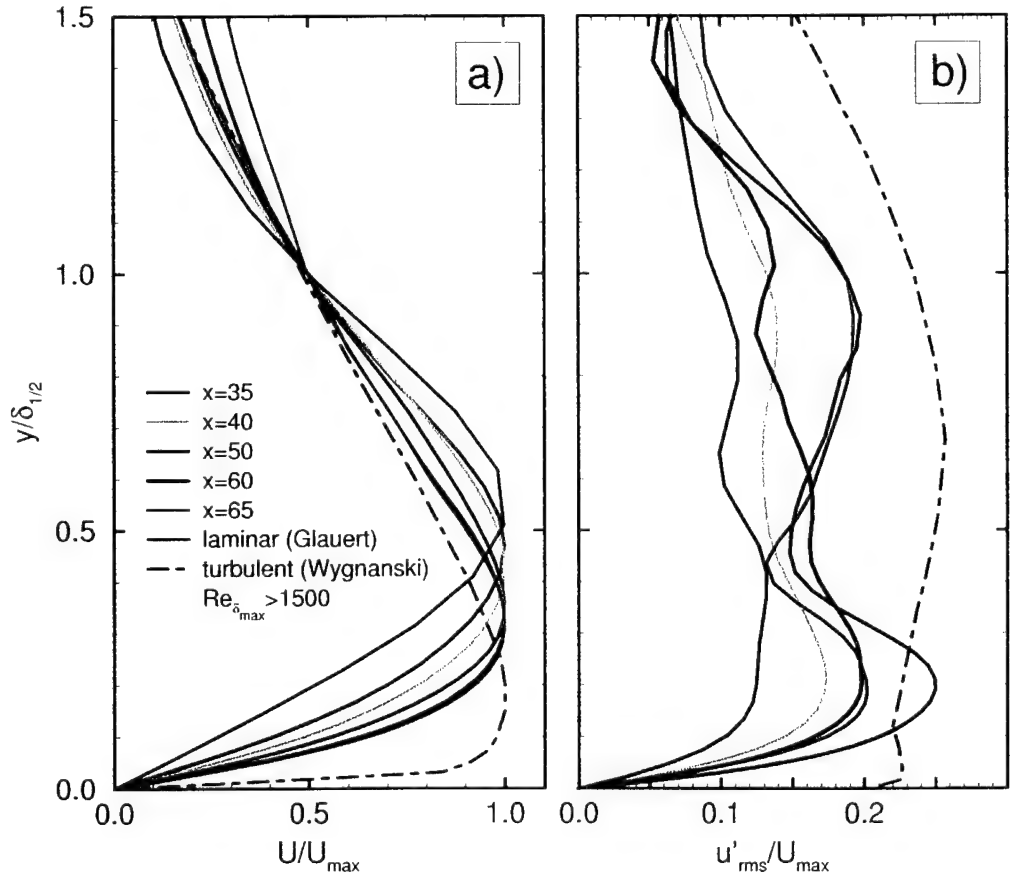

Figure 8: For the LES results shown in Figure 7: a) normalized meanflow velocity profiles, and b) rms–velocity profiles normalized with the half width and the local velocity maximum at five streamwise locations. Comparison with laminar profiles [similarity solution by Glauert (1956)] and with turbulent profiles [from experiments by Wygnanski et al. (1992)].

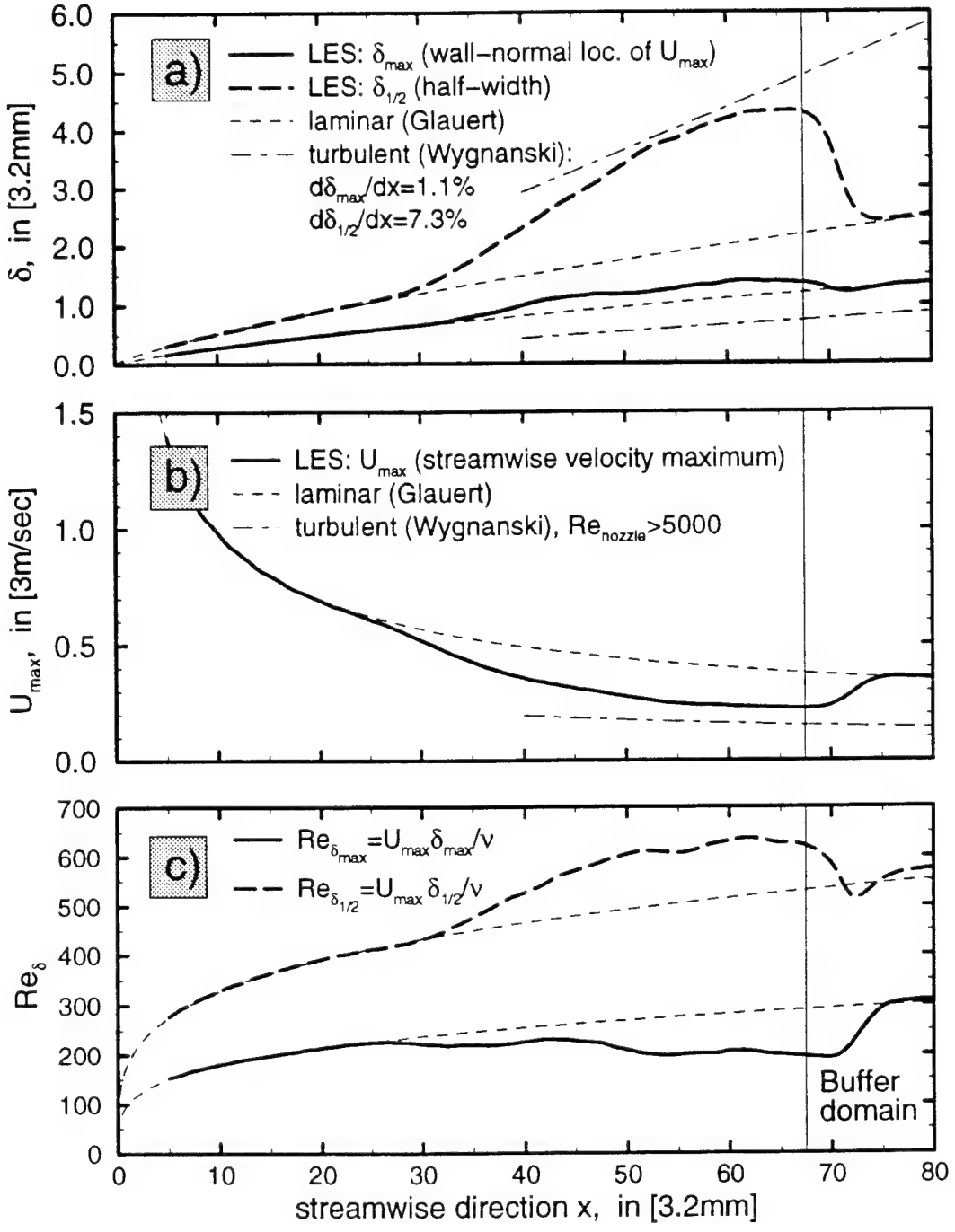

Figure 9: LES of bypass transition in a wall jet: a) streamwise development of the wall jet thickness (half width and location of velocity maximum, b) the local velocity maximum, and c) the local Reynolds numbers. Comparison with values for the laminar wall jet (Glauert 1956) and also with a fully turbulent wall jet [from experiments by Wygnanski et al. (1992); the experiments for the turbulent wall jet are at Reynolds numbers that are 10 times higher than those reached in the LES].

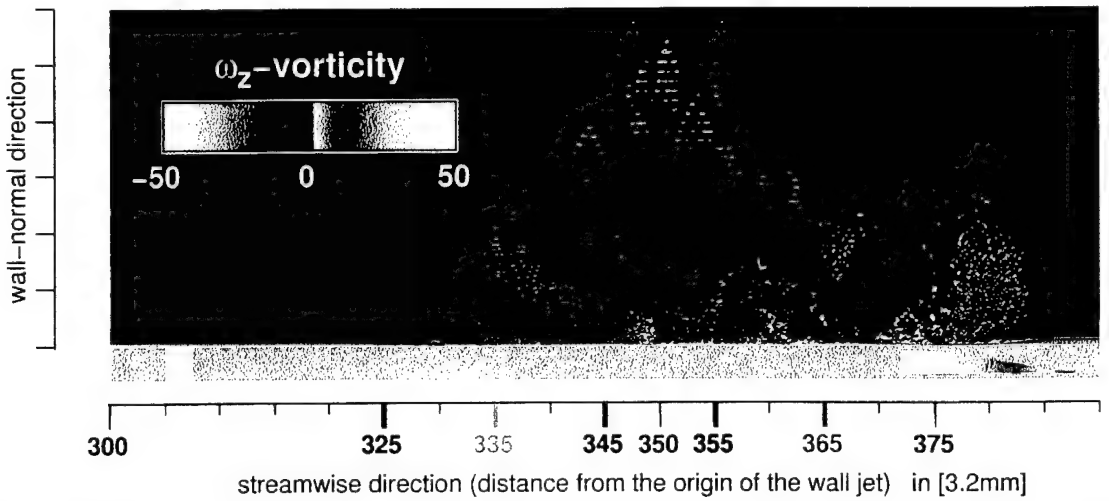

Figure 10: Bypass transition in a wall jet at higher Reynolds numbers (computed with our LES code). Shown are color contours of the two–dimensional Fourier component (k=0) of the spanwise vorticity. The flow is disturbed by random forcing (blowing and suction slot) in the first and in the second spanwise Fourier component (k=1,0).

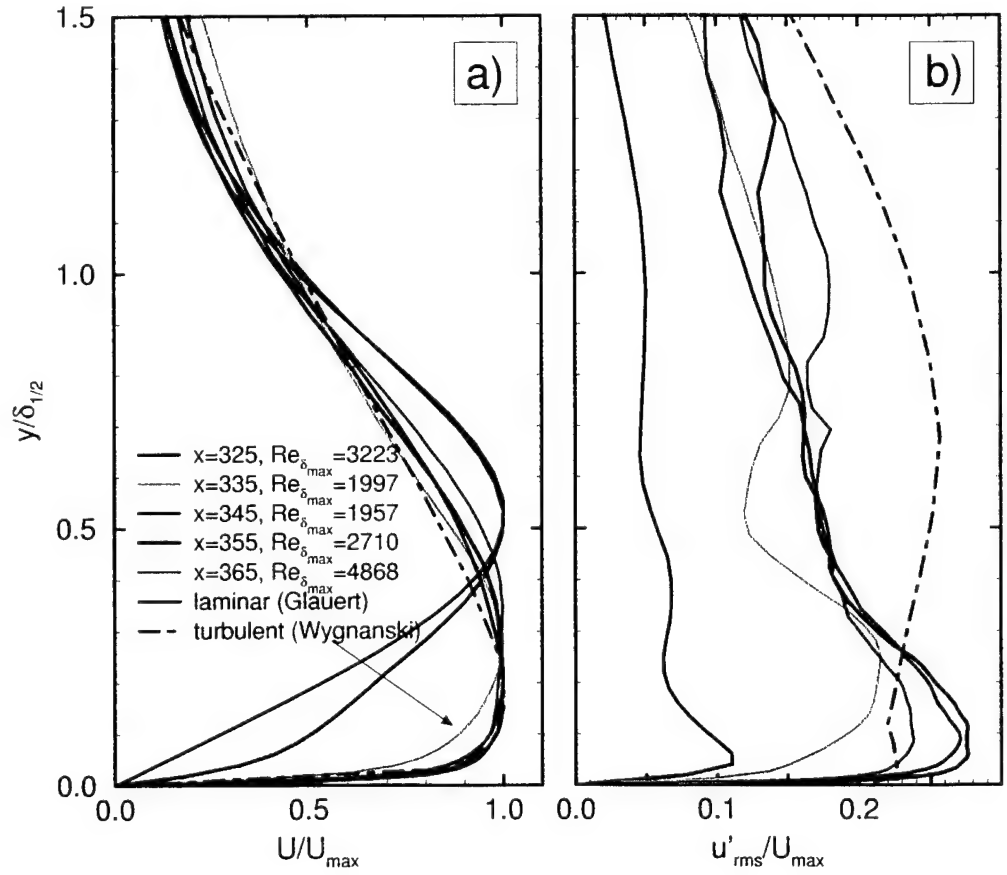

Figure 11: For the LES results shown in Figure 10: a) normalized meanflow velocity profiles, and b) rms–velocity profiles normalized with the half width and the local velocity maximum at five streamwise locations. Comparison with laminar profiles [similarity solution by Glauert (1956)] and with turbulent profiles [from experiments by Wygnanski et al. (1992)].

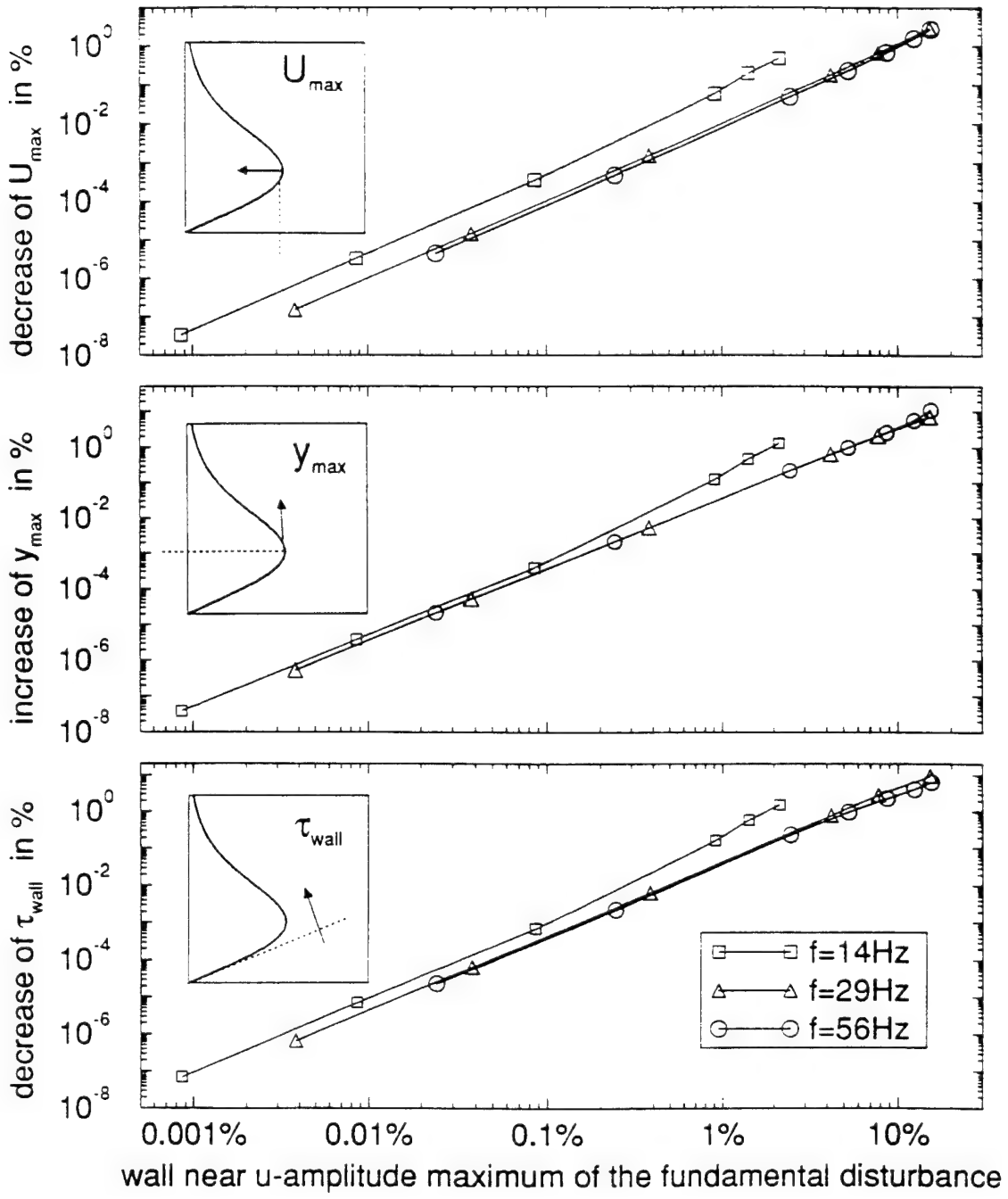

Figure 12: Influence of the disturbance level on the mean flow. The graphs from top to bottom show the decrease of the local u–velocity maximum, the increase of the half width of the wall jet, and the decrease of the wall shear as functions of the local u–amplitude maximum of the fundamental disturbance wave.

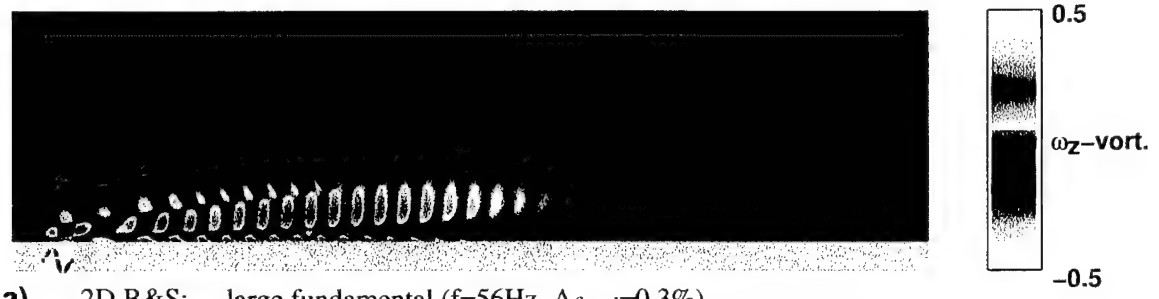

a) 2D B&S: large fundamental (f=56Hz, A_{fund}=0.3%)
+ small subharmonic (f=28Hz, A_{subh}=0.001%)

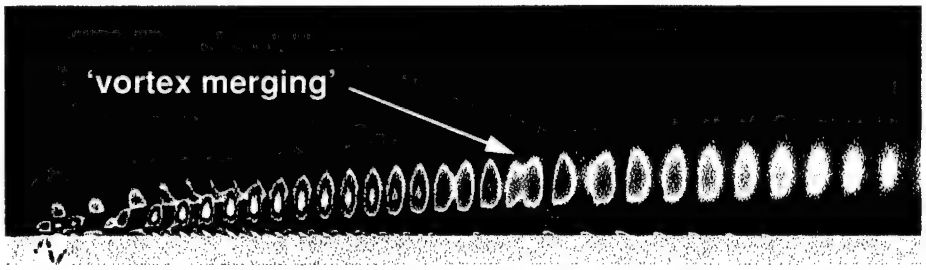

b) 2D B&S: larger fundamental (f=56Hz, A_{fund}=0.5%)
+ small subharmonic (f=28Hz, A_{subh}=0.001%)

Figure 13: Two–dimensional subharmonic resonances for large–amplitude forcing by blowing and suction. Shown are color contours of instantaneous spanwise vorticity (of the disturbance flow) for two different forcing levels: a) smaller forcing amplitude (A_{fund}=0.3%), b) larger forcing amplitude (A_{fund}=0.5%). In this case, merging of vorticity concentrations is observed when the flow is also forced with a very small subharmonic disturbance.

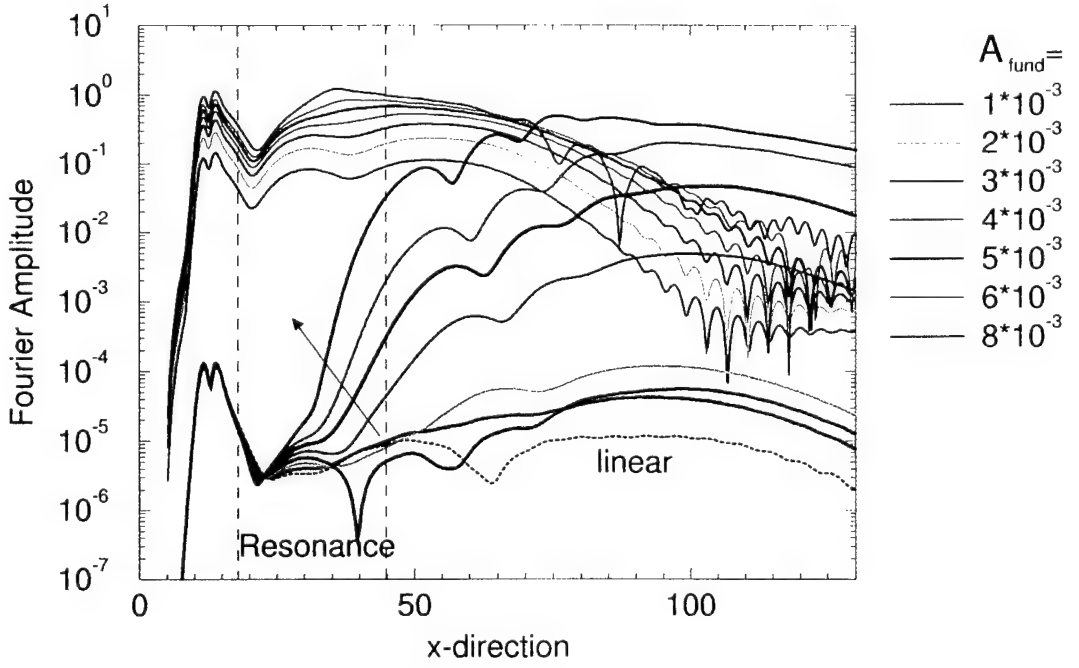

Figure 14: Dependence of the 2–D subharmonic resonance mechanism on the forcing amplitude of the fundamental. Shown are the Fourier amplitudes of the wall vorticity of the fundamental and of the subharmonic disturbance for six different forcing amplitudes of the fundamental.

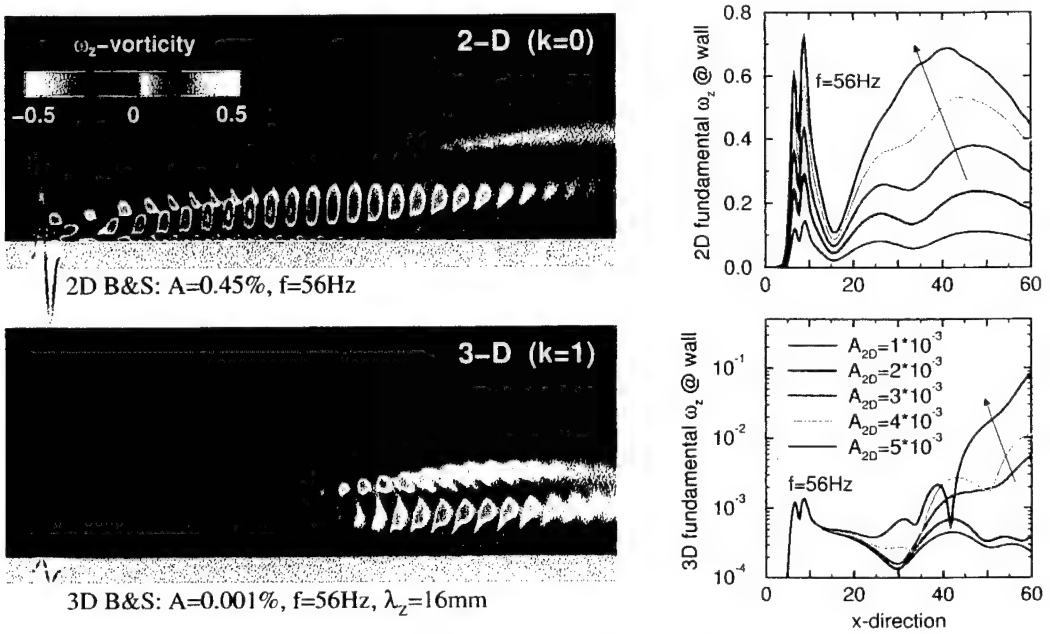

Figure 15: Results of a DNS for a three–dimensional **fundamental** resonance. The plots on the left display contours of instantaneous spanwise vorticity (disturbance flow). The top graph shows the 2–D Fourier component (k=0) with large–amplitude forcing at the fundamental frequency, the bottom graph shows the first spanwise Fourier component (k=1) with very small–amplitude forcing at the same frequency. The corresponding graphs on the right show the Fourier amplitudes of the wall vorticity for both components and for several forcing levels of the 2–D component.

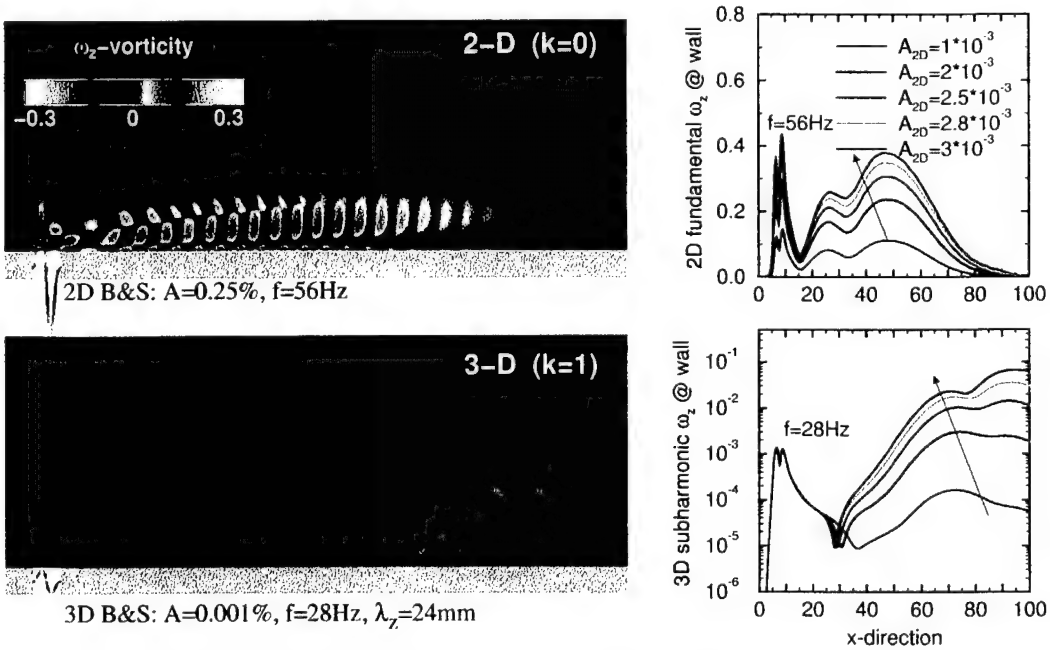

Figure 16: Results of a DNS for a three–dimensional **subharmonic** resonance. The plots on the left display contours of instantaneous spanwise vorticity (disturbance flow). The top graph shows the 2–D Fourier component (k=0) with large–amplitude forcing at the fundamental frequency, the bottom graph shows the first spanwise Fourier component (k=1) with very small–amplitude forcing at half that frequency. The corresponding graphs on the right show the Fourier amplitudes of the wall vorticity for both components and for several forcing levels of the 2–D component.

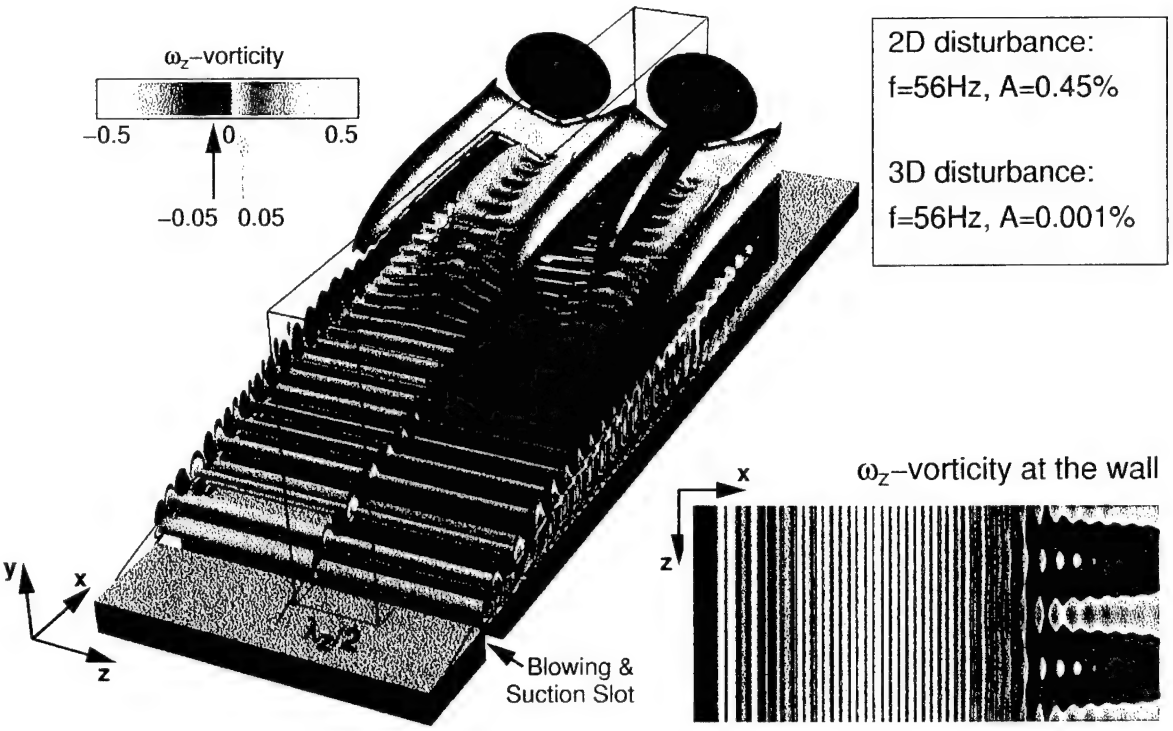

Figure 17: Results of a DNS for a three–dimensional **fundamental** resonance. Shown are iso–surfaces of the spanwise vorticity (left) and color contours of the spanwise wall vorticity (right).

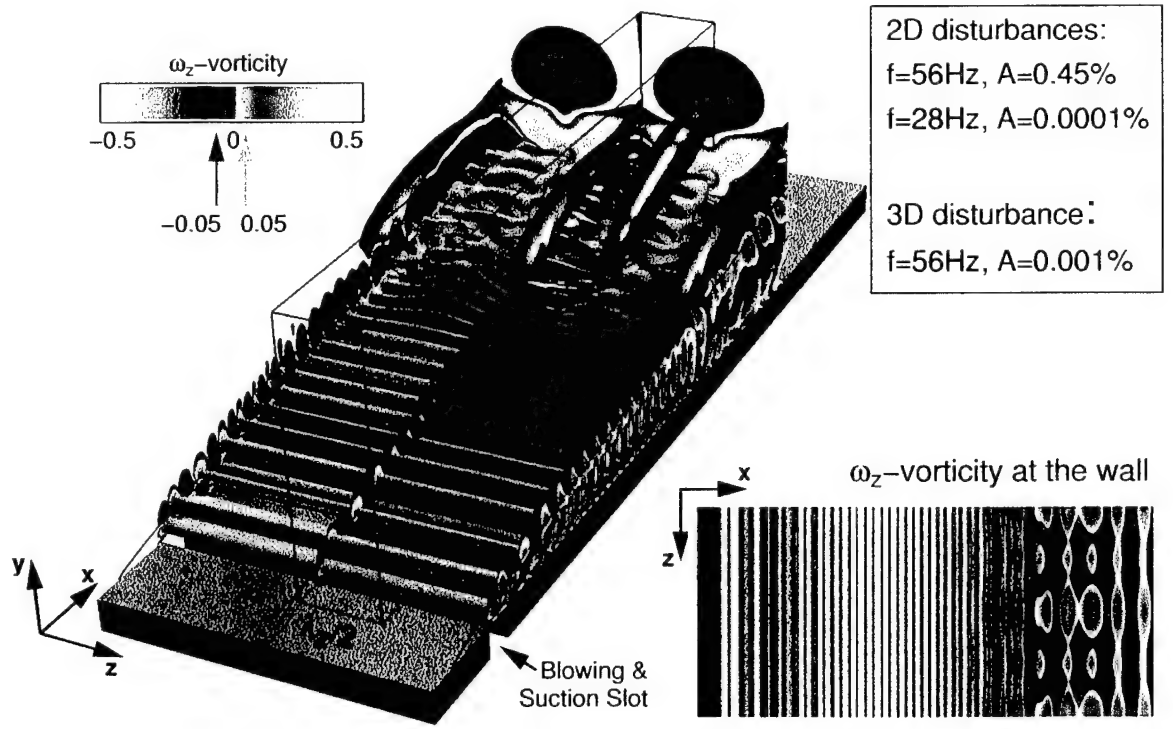

Figure 18: Results of a DNS for a three–dimensional **combination** resonance (3–D fundamental + 2–D subharmonic). Shown are iso–surfaces of the spanwise vorticity (left) and color contours of the spanwise wall vorticity (right).

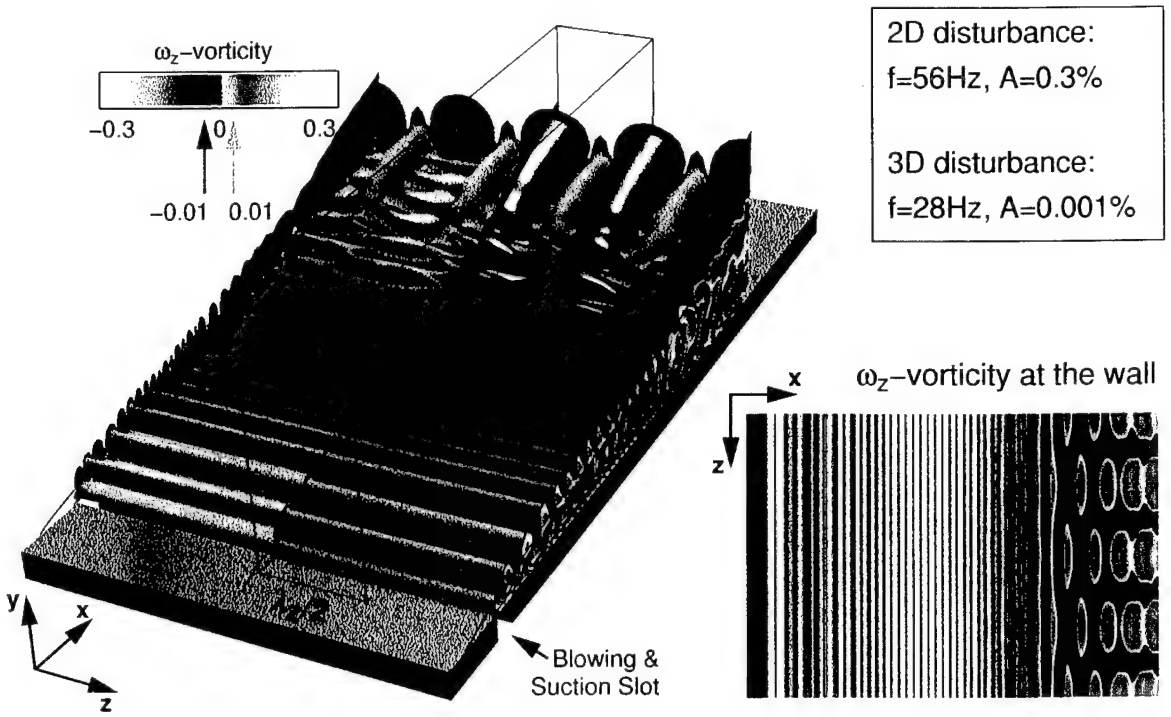

Figure 19: Results of a DNS for a three–dimensional **subharmonic** resonance. Shown are iso–surfaces of the spanwise vorticity (left) and color contours of the spanwise wall vorticity (right).

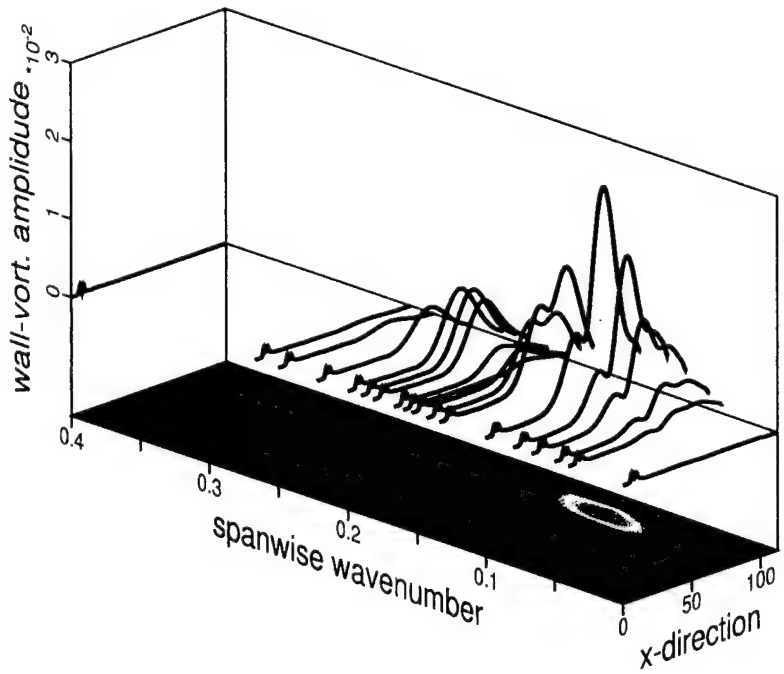

Figure 20: Dependency of the three–dimensional **subharmonic** resonance on the spanwise wave number. Shown are the Fourier amplitudes of the spanwise wall vorticity versus the streamwise distance and the spanwise wavenumber.

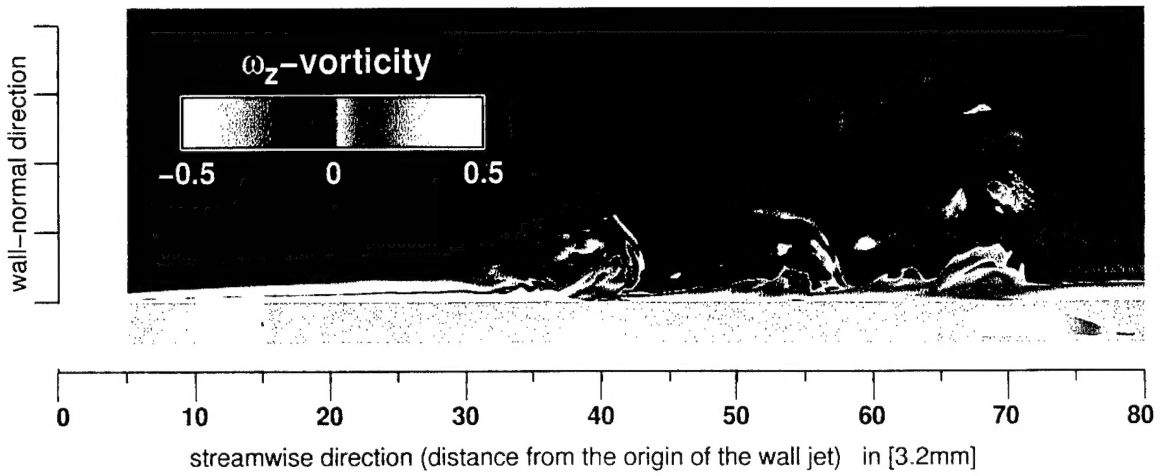

a) two–dimensional Fourier component (k=0)

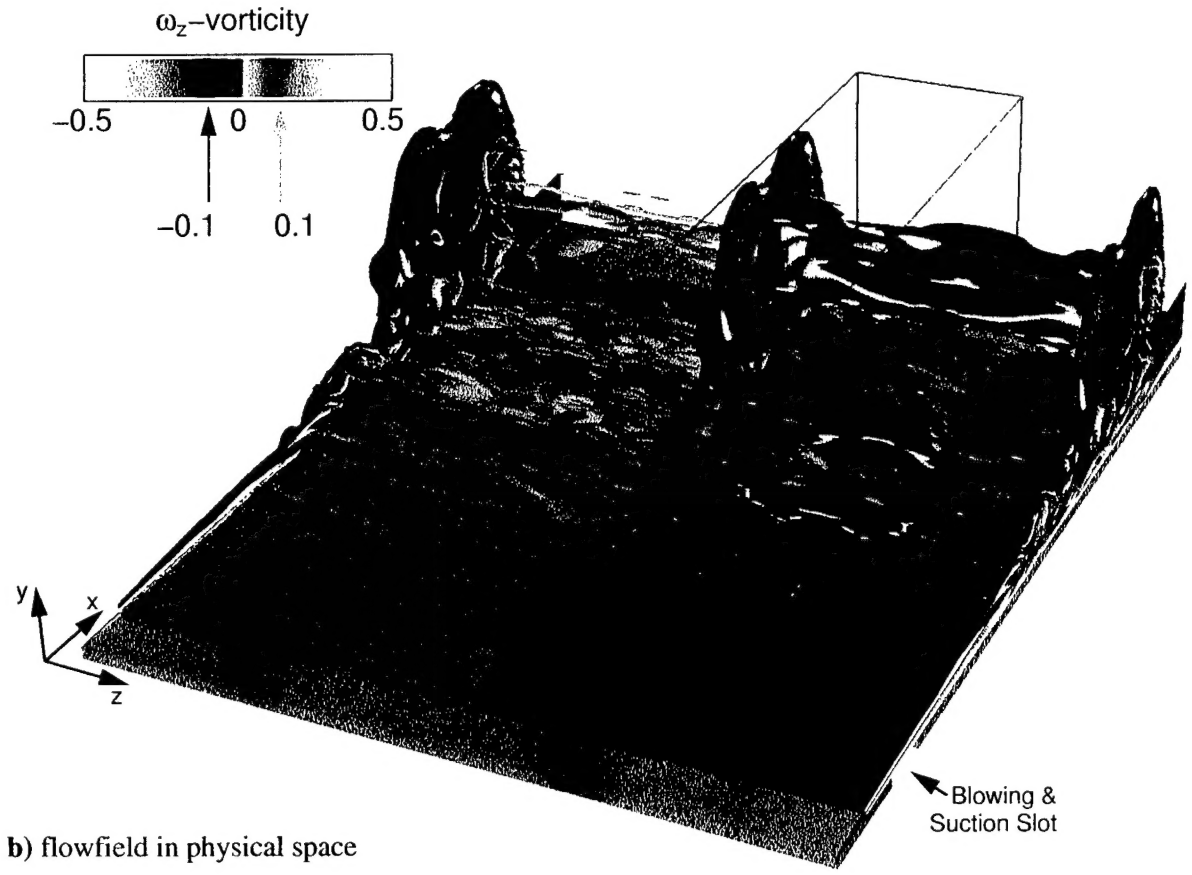

b) flowfield in physical space

Figure 21: Generation of two–dimensional coherent structures during bypass transition in a wall jet without external stream (computed with LES): a) color contours of the two–dimensional Fourier component (k=0) of the spanwise vorticity and b) iso–surfaces of the spanwise vorticity in physical space.The flow is disturbed by random blowing and suction in the first and in the second spanwise Fourier component (k=1,2).

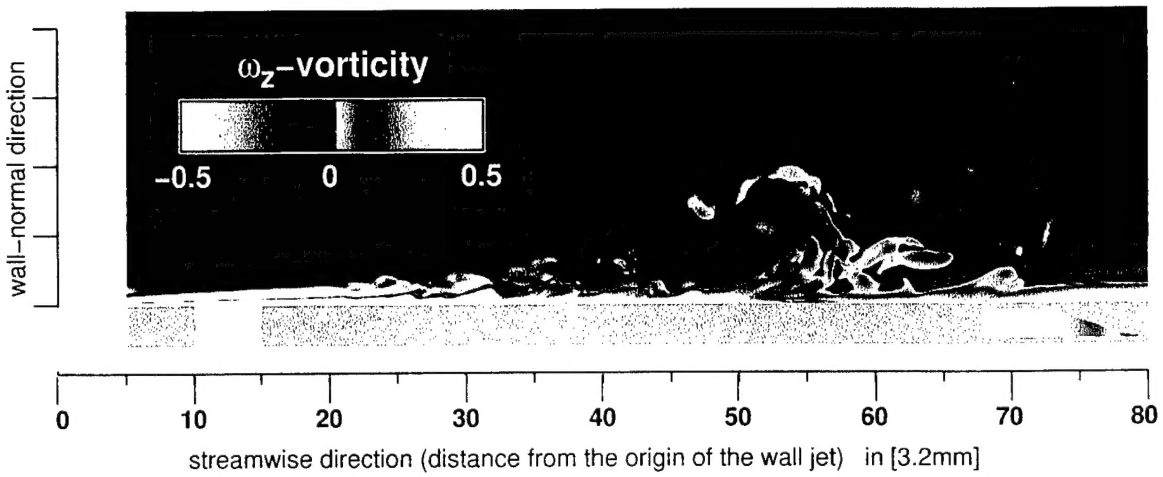

a) two–dimensional Fourier component (k=0)

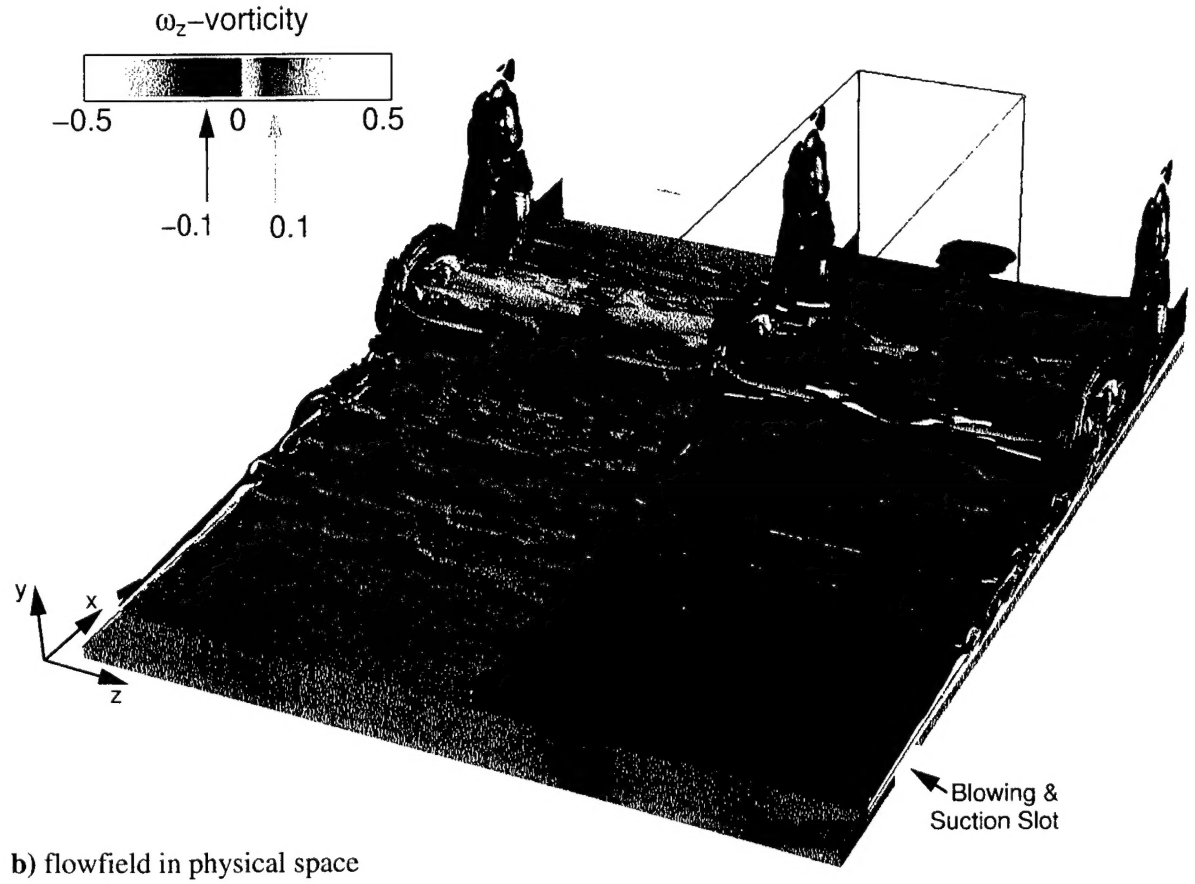

b) flowfield in physical space

Figure 22: By–pass transition in a wall jet with a moderate **external stream** component (computed with LES): a) color contours of the two–dimensional Fourier component (k=0) of the spanwise vorticity, and b) iso–surfaces of the spanwise vorticity in physical space.The flow is disturbed by random blowing and suction in the first and in the second spanwise Fourier component (k=1,2).

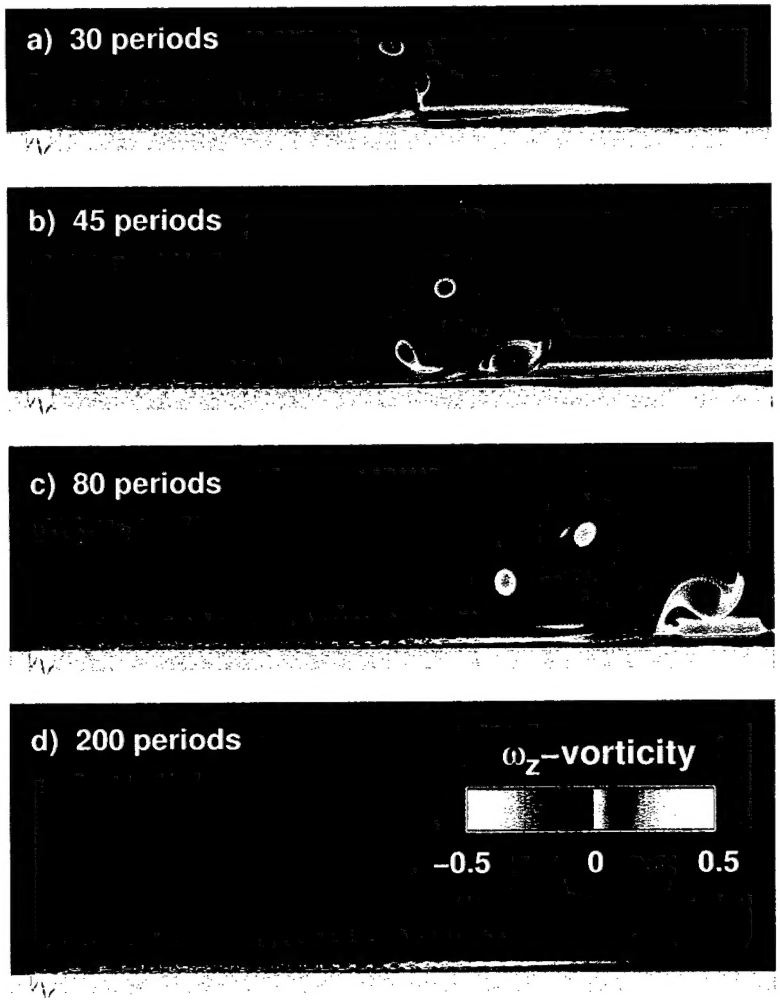

Figure 23: Startup of disturbing a wall jet with an **external stream** component by blowing and suction. Shown are color contours of instantaneous spanwise vorticity (disturbance flow) at different time instants.

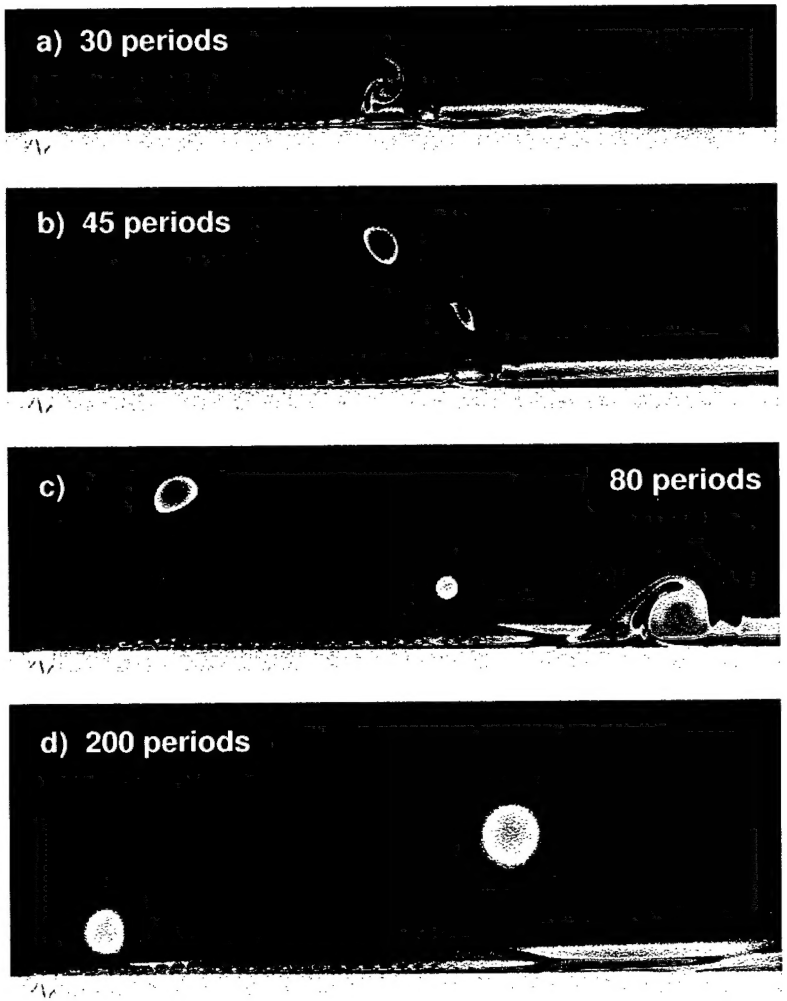

Figure 24: Startup of disturbing a wall jet without an external stream component by blowing and suction. Shown are color contours of instantaneous spanwise vorticity (disturbance flow) at the same time instants as for the case shown in Figure 23.

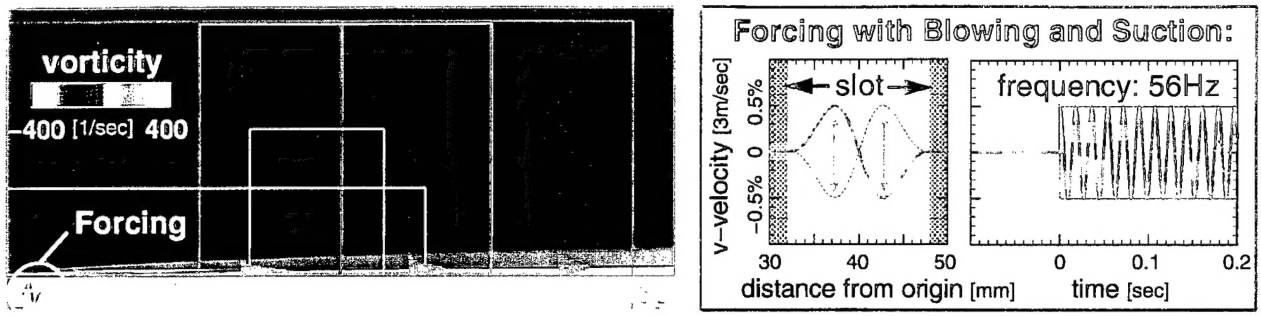

Figure 1: Computational domain with base flow (Glauert's similarity solution) and method of forcing.

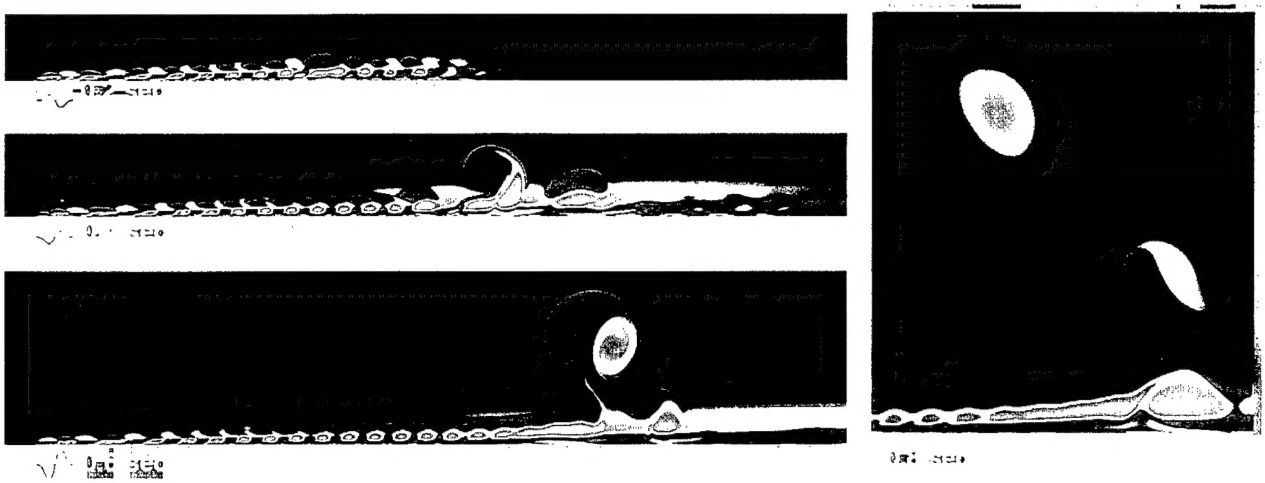

Figure 2: Time sequence for the disturbance flow during startup of forcing with blowing and suction.

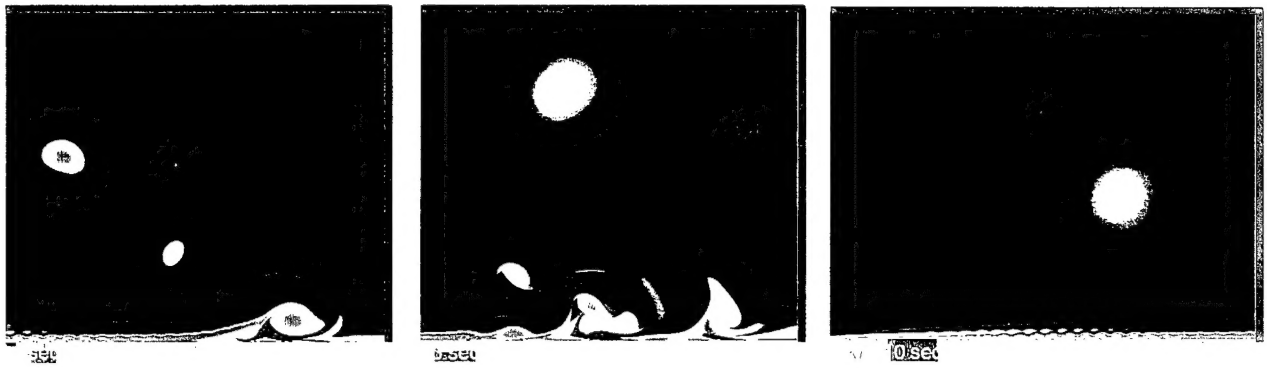

Figure 3: Snapshots of the total flow (base flow + disturbance flow) at three instants in time (1, 3, 10 sec).

VORTEX MOTION IN AN UNSTEADY FORCED WALL JET

Submitted by Stefan Wernz and Hermann F. Fasel
(University of Arizona)

Transitional wall jets are being investigated[1] using Direct Numerical Simulations (DNS). In the present simulation, the two–dimensional vorticity transport equation in disturbance flow formulation is solved numerically over the computational domain shown in figure 1 ($Re_{\delta 0.5}$=277–701). The base flow for the computation is given by Glauert's similarity solution, as shown in figure 1 using color contours of spanwise vorticity. By forcing the wall jet with periodic blowing and suction through a slot in the wall (figure 1) traveling disturbance waves are introduced into the flow. During startup of periodic forcing with large amplitudes, a series of mergings of subsequent vorticity concentrations occurs within the disturbance waves (figure 2). These mergings are manifestations of a subharmonic resonance between the fundamental disturbance wave (f=56Hz) and disturbance waves with lower frequencies that are generated momentarily by the sudden startup of forcing. This secondary instability process leads to an accumulation of vorticity within one pair of vorticities that is eventually ejected from the wall jet layer into the ambient fluid. By mutual induction this mushroom shaped vortex pair travels upstream and then interacts repeatedly with the wall jet. As a consequence, a very complex flow pattern develops (figure 3) that is sensitive to initial conditions and, in the present two–dimensional calculation, persists for about 30 seconds before the flow reaches a time–periodic state. In three–dimensional computations, breakdown to turbulence takes place shortly after the first vortex pair is ejected. This research is funded by AFOSR under contract number F49620–94–1–0208.